MAGMA CHAMBER DYNAMICS

AT MOUNT EREBUS VOLCANO, ANTARCTICA:

DETERMINED USING VOLATILE RADIONUCLIDE EMISSIONS

Jessie Larkin Crain

Independent Study Submitted in Partial Fulfillment
of the requirements for the Degree of
Masters of Science in Geology

New Mexico Institute of Mining and Technology

Socorro, New Mexico
August 2002

TABLE OF CONTENTS

ABSTRACT

Mount Erebus, a continuously active volcano located on Ross Island, Antarctica, hosts a permanent, convecting lava lake and provides an ideal location to study direct gas emissions to the atmosphere. Measurements of the long-lived volatile uranium daughters ^{210}Pb, ^{210}Bi, and ^{210}Po in the volcanic plume are used to estimate recharge rates and volumes of the degassing magma chamber. During the austral summer field seasons in 1999, 2000, and 2001, radionuclide samples were collected on the crater rim. These samples were analyzed for ^{210}Pb, ^{210}Bi, and ^{210}Po using alpha and beta counting techniques. Concentrations of these species in the plume vary widely, dependent on the strength of the plume at the sample site on a given day.

Activity ratios allow a comparison of radionuclides in the plume from one year to the next. In 1999, the mean ($^{210}Po/^{210}Pb$) activity ratio was 58 and the mean ($^{210}Bi/^{210}Pb$) was 18. In 2000, the mean ($^{210}Po/^{210}Pb$) ratio was 68; the mean ($^{210}Bi/^{210}Pb$) was 19. In 2001, the mean ($^{210}Po/^{210}Pb$) was 47. No ($^{210}Bi/^{210}Pb$) ratio is available for 2001. Using these activity ratios in a degassing model developed by Gauthier et al. (2000), it is possible to calculate recharge rates (per unit time) and residence times for the degassing magma. The recharge rate slowed from 1.8 to 0.6 $year^{-1}$ during 2000, corresponding to residence times increasing from 203 to 606 days. In 2001, the recharge rate sharply increased to 21 $year^{-1}$, which corresponds to a residence time of 17 days. This increase in recharge in 2001 could be the result of an intrusion of new magma to the system over the course of 2000 and 2001. During 2000 and the beginning of 2001, seismic tremor and mild deformation indicated that magma was moving at a depth of 5 – 7 km. In 2001, a lower ($^{210}Po/^{210}Pb$) activity ratio reflected degassing of this fresh magma.

Assuming a constant volume of magma in the system, the change in residence time seems to indicate a yearly change in mass flux into the system, which slowed from 1999 to 2000 and increased again in 2001. If the new magma entered the deep system in 2000, the evidence of it in the shallow degassing system at the end of 2001 supports Klimasauskas' (1995) conclusion that the system experiences large-scale cycling over a 2 – 3 year period.

Another important issue surrounding Mount Erebus is the volcano's impact on the local environment. We use ^{210}Po as an atmospheric tracer to estimate the influence of the Erebus plume on levels of SO_4^{2-} and ^{210}Pb measured at the South Pole. Comparing ratios of $SO_4^{2-}/^{210}Po$ and $^{210}Pb/^{210}Po$ at both locations, we estimate that Erebus contributes ~16-28% of the SO_4^{2-} and ~0.2-0.4% of the ^{210}Pb. The low percentage of ^{210}Pb is significant, indicating a much higher level of anthropogenic lead in the Antarctic atmosphere than previously thought (Zreda-Gostynska et al., 1997).

ACKNOWLEDGEMENTS

I would like to thank my advisor, Philip Kyle, for his support at every stage of this project. I would also like to thank Andrew Campbell and Nelia Dunbar for their work as members of my committee. Tremendous assistance in the field came from Philip Kyle, Bill McIntosh, Nelia Dunbar, Jean Wardell, Rick Aster, Rich Karstens, Rich Esser, Jeff Johnson, Noel Barstow, Jean Roberts, Tim Vermaat, Emily Desmarais, Tina Calvin, Forrest McCarthy, Chas Day, Homer, Bo, and Cmdr. Laboratory assistance was given by Terry Thomas at the New Mexico Bureau of Geology and Mineral Resources and by Marie-Françoise Le Cloarec at the Laboratoire des Sciences du Climat et de l'Environnement, CNRS-CEA and Pierre-Jean Gauthier at the Universite Blaise Pascal. Drs. Le Cloarec and Gauthier were also extremely instrumental in my overall understanding of this project and helped me work out many of the problems along the way. Finally, my everlasting gratitude to Benjamin Rebach, who survived three years in the desert so that this work could be completed.

This work was funded through a fellowship from the New Mexico Tech Graduate Office and by a National Science Foundation, Office of Polar Programs grant to Philip Kyle.

INTRODUCTION

One of the fundamental problems in the study of volcanoes and their eruptive behavior is determining the nature and dynamics of the associated magmatic system. Of great importance is knowing the size and depth of a magma chamber and its recharge rate. An understanding of magma chambers can be obtained from geochemical models which examine the gases emitted at a volcano from an underlying magma system. For passively degassing volcanoes, it is often relatively easy to sample volcanic gases, either directly at the crater rim of the volcano or near the vent using airborne techniques. The sampled gases can be studied using a variety of techniques in order to determine impact of volcanism on the atmosphere, as well as to provide insight into possible eruptive activity. In addition to conventional gas studies, investigation of the ^{238}U decay series provides the means to develop geochemical models of volatile origin, exsolution and degassing. In an undisturbed magmatic system, all daughters in the U-series are in radioactive equilibrium; their decay rates are equal. When a process such as degassing occurs, the more volatile elements (Rn, Pb, Bi, and Po) are lost from the system, creating disequilibrium in the isotopic ratios of the appropriate nuclides (Lambert et al., 1986). The timing of the processes responsible for the disequilibrium can be determined from the degree of disequilibrium.

^{210}Pb, ^{210}Bi, and ^{210}Po are the longest lived daughters in the ^{238}U decay series that are volatile at magmatic temperatures. Because of their different half-lives and degrees of volatility, activity ratios of these species are useful for understanding magmatic processes that occur on timescales of days, months and years (Gauthier et al., 2000; Lambert et al., 1986; Le Cloarec and Lambert, 1993). These processes include recharge

rates in the magma chamber, the volume of the degassing cell, and the escape time of gas bubbles from the melt.

To gain a better knowledge of the magma system at Mount Erebus volcano, Antarctica, we collected gas and aerosol samples during December 1999, 2000, and 2001 in order to determine emissions of SO_2 and (^{210}Pb), (^{210}Bi), and (^{210}Po) (where isotopes enclosed in brackets refer to their activities) in the volcanic plume. Using the (^{210}Po/^{210}Pb) and (^{210}Bi/^{210}Pb) activity ratios, we applied a degassing model developed by Gauthier (2000) to the Erebus magmatic system. The principle objective was to determine the recharge rate and volume degassing system.

In addition to the uses in understanding magma chamber dynamic, U-series daughters, especially ^{210}Po, can be used as atmospheric tracers (see Arimoto et al., 2001; Nho et al., 1996, Su and Huh, 2002). We can compare (^{210}Po/^{210}Pb) and (^{210}Po)/S ratios at Erebus with similar measurements made at the South Pole and estimate the contribution of the Erebus plume to levels of SO_4^{2-} and ^{210}Pb in the Antarctic atmosphere.

VOLCANIC ACTIVITY OF MOUNT EREBUS

Mount Erebus is a 3794-m high active volcano located on Ross Island, Antarctica, which hosts a persistent convecting lake of anorthoclase phonolite magma. The eruptive activity at Mt. Erebus is dominated by strombolian eruptions, which generally occur several times per day. The Erebus crater is made up of a large Main Crater, approximately 500 m by 600 m, which contains at the northeastern end a smaller Inner Crater, approximately 250 m in diameter. The Main Crater floor lies 120 m beneath the crater rim, with the Inner Crater floor 100 m below the main floor. The Inner Crater contains the phonolite lava lake that was first observed in 1972 (Giggenbach et al., 1973).

At the time of sampling in 1999, the lava lake was approximately 15 m in diameter. The convecting lava lake allows gases to escape directly from the magma to the atmosphere without alteration from wall-rock interactions, making Mount Erebus an ideal location to sample magmatic gases.

The primary source of the phonolite at Mount Erebus may be a mantle plume approximately 40 km in diameter in which low degrees of partial melting generate a parental basanite magma (Kyle et al., 1992). Mount Erebus and the plume are situated at the southern end of the Terror Rift which lies within the Victoria Land basin (Cooper et al., 1987; Kyle, 1990). The distribution of volcanic centers surrounding Erebus suggests crustal doming resulting in radial fractures at ~120° to each other (Kyle and Cole, 1974). Doming is an indication of the onset of plume upwelling. The oldest rocks at Mount Erebus have been dated to 1.13 Ma (Esser et al., submitted). The anorthoclase phonolite magma is a 23.5% residual liquid formed by fractional crystallization of the parental basanite magma (Kyle et al., 1992). The phonolite is the most evolved and alkaline member of the Erebus lineage, which includes basanite/tephrite, phonotephrite, and tephriphonolite lavas (Kyle, 1977, Kyle et al., 1992, Dunbar et al., 1994). The phonolite lavas and pyroclastic rocks are composed of black vesiculated and pumiceous glass and 25-35% large (up to 10 cm) anorthoclase feldspar with minor smaller crystals of olivine, clinopyroxene, pyrrhotite, magnetite, and apatite (Kyle et al., 1992). The magma has an average density of 650 – 1300 kg/m^3 (Dibble, 1994), with an average melt density of 2700 kg/m^3 (Dunbar et al., 1994).

The eruptive activity at Mount Erebus over the past two decades has been well-documented using seismic methods. Kaminuma (1994) surveyed seismic activity at

Mount Erebus during 1981 – 1990. He identified four phases of seismic activity during this period, each relating to a different phase of volcanic activity. From December 1980 to September 1982, there were 50 – 100 daily earthquakes. From October 1982 to August 1984, earthquake activity increased to over 100 earthquakes per day, with several earthquake swarms each year, lasting between 36 hours and 15 days with up to 2888 earthquakes in one day. During September to December 1984, Mount Erebus had a significant increase in the size and frequency of Strombolian eruptions (Dibble et al., 1988, Caldwell and Kyle, 1994). From 1985-1990 seismic activity declined sharply, with fewer than 20 earthquakes per day. Primary eruptive activity between 1994 and 1999 included 2 to 6 small Strombolian eruptions per day, rare ash eruptions, and infrequent periods of harmonic tremor (Rowe et al., 2000). Rowe et al. (2000) explain shallow explosions (Strombolian eruptions and swarm activity) as the passive degassing of the deep magma and occasionally the result of landslides of rock, snow, and ice onto the lava lake from the crater walls. Tremor occurs during periods of magma movement, such as a dike injection in October, 1982. Tremor may also be the result of changes in the size of the resonant chamber or changes in the volatile content or distribution within the magma (Chouet, 1996; Garces et al., 1998; Hagerty et al., 1997).

Sulfur dioxide emission rates have been measured nearly every year since December 1983. Emission rates vary through time and generally correlate with the exposed surface area of the lava lake (Kyle et al., 1994). In 1983, Rose et al. (1985) measured SO_2 fluxes of 230±90 Mg/day (84 Gg/year). This measurement preceded by less than a year the dramatic increase in eruptive activity in the austral spring of 1984. Kyle et al. (1994) reported more recent SO_2 fluxes ranging from 6 to 84 Gg/year (16 –

230 Mg/day) between 1986 and 1991. The current daily average flux is 50±10 Mg/day SO_2 (P. Kyle, pers. comm.). Sulfur dioxide flux at Erebus is fairly low in comparison to other active volcanoes (see Andres, 1998 for SO_2 fluxes from 49 active volcanoes). Halogen emissions are relatively high in comparison to SO_2 fluxes, with HCl emissions from 6.9 to 13.3 Gg/year (~19 – 36 Mg/day) and HF emissions from 4.0 to 6.0 Gg/year (11 – 16 Mg/day) (Zreda-Gostynska et al., 1997). Klimasauskas (1985) interpreted variations in S, F, and Cl values to indicate large-scale convection and possible deep recharge of the magma chamber.

Eschenbacher (1998) measured H_2O, CO_2, and trace elements in melt inclusions from lavas and pyroclasts spanning the compositional range of rock types on Erebus. The melt inclusions were anorthoclase-hosted in the phonolite and olivine-hosted in all other compositions. Eschenbacher reports melt inclusions from a basanite to have 1.15 to 1.75 wt% H_2O; 0.5 wt% H_2O in the tephriphonolite and ~0.1 wt % H_2O in all other rock types. Pre-eruptive CO_2 contents measured in melt inclusions were 4000-7300 ppm in the basanite and <2000 ppm in olivines from other compositions. Concentrations of S in melt inclusions range from 2500 ppm in the basanite to 400 ppm in the phonolite; F in melt inclusions ranges from 1600 to 2600 ppm across all compositions; and Cl in melt inclusions ranges from 740 ppm in basanite to 1500 ppm in phonolite. The total pre-eruptive volatile content is estimated at 2.5% in the basanite and 0.63% in the tephriphonolite. Based on the CO_2 and H_2O concentrations of the melt inclusions in basanite samples, Eschenbacher (1998) determined a vapor saturation pressure of 3 – 4.5 kbar, which indicates an inclusion trapping depth of 8 – 13 km.

Several researchers have made preliminary analyses of uranium-series radionuclides at Mount Erebus. Polian and Lambert (1979) measured activities of radon daughters in the Erebus plume during the 1977-78 field season. They observed (^{210}Pb), (^{210}Bi), and (^{210}Po) at 0.3 Bq/m^3, 3.1 Bq/m^3, and 9.3 Bq/m^3, respectively, with (^{210}Bi/^{210}Pb) = 10.3 and (^{210}Po/^{210}Pb) = 31. K. Sims (pers. comm.) measured (^{210}Pb) = 0.08 Bq/g and (^{226}Ra) = 0.087 – 0.088 Bq/g in a lava bomb erupted in 1984.

URANIUM DECAY

The ^{238}U decay series is the longest radioactive decay chain in nature (Figure 1). The ^{238}U parent makes up 99.27% of natural uranium (Ivanovich, 1992) and decays to ^{206}Pb. The main series progresses through eight alpha and six beta decays. A decay chain behaves in such a way that all members of the series reach radioactive equilibrium with one another in five half-lives of the longest-lived intermediate nuclide (Condomines et al., 1988). The longest-lived daughter in the ^{238}U decay series is ^{230}Th, which has a half-life of 75,400 years; therefore, the ^{238}U series reaches equilibrium in ~4x10^5 years. The activity, or decay rate, of a radionuclide is a function of the number of atoms of the species present in a sample and the decay constant for that species. The activity describes the number of radioactive decays of a particular species over a given time. When the decay series reaches radioactive equilibrium, the activity of each parent equals the activity of each daughter. When all activities are equal and hence the decay chain is in radioactive equilibrium, it behaves as if a single isotope with the half-life of the parent of the decay series is decaying to the final daughter nuclide ^{206}Pb.

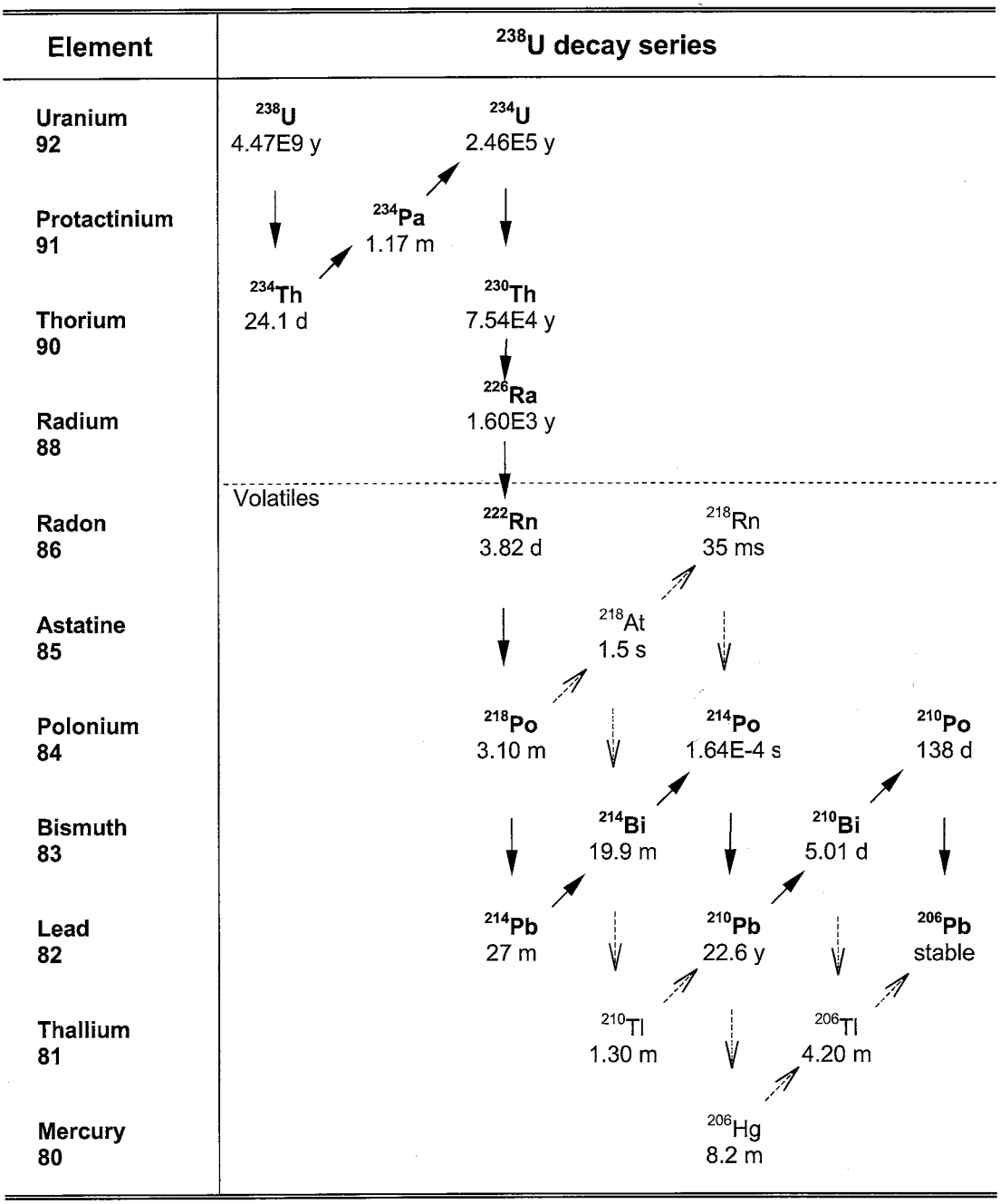

Figure 1. ^{238}U decays through 8 alpha decays and 6 beta decays to ^{206}Pb. A small percentage of decays result in branched decay of the chain. The main decay chain is shown in bold type. Isotopes below the dashed line are volatile at magmatic temperatures. y: year; d: day; m: minute; s: second; ms: millisecond. All half-lives and decay percentages from Parrington et al. (1996).

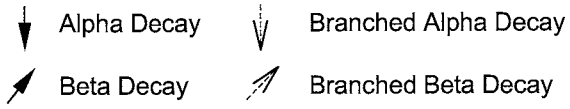

MODEL OF MAGMA DEGASSING

Processes such as melting, crystallization, and degassing can cause fractionation in the uranium-decay series (Condomines et al., 1988; Gauthier and Condomines, 1999; Gauthier et al., 2000; Lambert et al., 1986; Oversby and Gast, 1968; Volpe and Hammond, 1991; Williams and Gill, 1989; Williams et al., 1986). When a species is preferentially removed during one of these processes, disequilibrium is created in which the parent and daughter activities are no longer equal. Measuring the disequilibrium that results in the long-lived volatile daughters of the uranium-decay series from fractionation due to degassing allows investigation of the timescales of shallow magmatic processes and degassing processes (Gauthier et al., 2000; Lambert et al., 1986; Le Cloarec et al., 1986). During degassing, the volatile nuclides ^{222}Rn, ^{210}Pb, ^{210}Bi, and ^{210}Po form halides and sulfides that may then partition into an H_2O-, CO_2-, H_2S- or SO_2-dominated gas phase, if one is present in the melt (Gauthier et al., 2000). Using the assumption that the uranium-decay series is in equilibrium in the deep magma, a disequilibrium measured in the gas phase is evidence of a process in the shallow magma that causes fractionation (Gauthier et al., 2000; Lambert et al., 1986). The disequilibrium can be measured if this fractionation happened within five half-lives of one of these volatile species.

Using these principles, Gauthier et al. (2000) developed a model of magma degassing based on the earlier models of Lambert et al. (1986) and Pyle (1992). This new model relies on a steady-state open system, in which the influx of new magma, ϕ_0, is balanced by the output flux of degassed lava, ϕ_L, and a gaseous phase, ϕ_G. This balanced magma flux allows the system to maintain a constant mass of magma, M. The influx magma (ϕ_0) has a pre-eruptive volatile content, that will eventual exsolve to form the

gaseous component ϕ_G. The model also assumes that any lava erupted from the system is of the same composition as the magma that remains in the chamber.

Gauthier et al. (2000) use a mass balance equation to describe the system in terms of radioactive decay and mass transfer. By substituting known parameters for the fluxes, they were able to arrive at an equation in which the only unknown was magma chamber recharge. This final equation is:

$$\left(\frac{Po}{Pb}\right)_G = \frac{\left[\frac{\phi_0}{M}\left(\alpha+\frac{1-\alpha}{D_{Pb}}\right)+\frac{\lambda_{Po}}{D_{Bi}}\left(\frac{\frac{\lambda_{Bi}}{D_{Pb}}+\frac{\phi_0}{M}\left(\alpha+\frac{1-\alpha}{D_{Pb}}\right)}{\frac{\lambda_{Bi}}{D_{Bi}}+\frac{\phi_0}{M}\left(\alpha+\frac{1-\alpha}{D_{Bi}}\right)}\right)\right]}{\left[\frac{\lambda_{Po}}{D_{Po}}+\frac{\phi_0}{M}\left(\alpha+\frac{1-\alpha}{D_{Po}}\right)\right]},$$

where ϕ_0/M is the recharge rate of the degassing magma volume per unit time, α is the pre-eruptive volatile content, M is the mass of degassing magma, and D is the partition coefficient of a particular species between the gas and liquid phases. The full derivation of this equation can be found in Gauthier et al. (2000).

METHODS

SO_2 and radionuclide samples were collected on the northeast edge of the Erebus crater rim during 10 days in December 1999. Radionuclide samples were also collected at the same site in December 2000 and 2001. Following collection, radionuclide activity on each filter was measured with α and β counting. Sulfur concentration was measured on impregnated alkali filters using ion chromatography. Glass and mineral separates from a bomb erupted in December 2000 were analyzed for ^{210}Po by α-spectroscopy and for ^{210}Pb by gamma counting as a step in determining the Po and Pb emanation coefficients.

Sampling and Impregnated Filter Preparation

Radionuclide samples were collected on Poelmann-Schneider blue cellulose filters. The filters were held in a custom-made filter holder giving an exposed filter ~6 cm in diameter. In 1999, the volcanic plume was drawn through the filters using a 120 volt generator-powered Gast Regenair R1102 rotary pump operating at a flow rate of 20 m^3/hr. (Appendix B contains details of the calibration of the pump). In 2000 and 2001, samples were collected using a battery-powered HI-Q CF-18V fan pump at a flow rate of 5-10 m^3/hr. After sampling, the filters were stored unfolded in cellophane bags. They were kept frozen until shipped by air courier to the CNRS laboratory in Gif-sur-Yvette, France, where the samples were analyzed within ~ two weeks of sampling.

Aerosols and acid gases in the volcanic plume were sampled using impregnated cellulose filters. Samples were collected using flow rates of ~1.1m^3/hr generated by battery-operated 12 volt vacuum pumps with attached flow meters. The filters were

treated with basic solutions which react with and trap SO_2 as the volcanic plume was drawn through the filter. 47 mm Whatman 41 filters were impregnated with one of three basic solutions: 3M LiOH, 4M NaOH, or 1M Zn Acetate. The solutions were prepared by combining ^{7}Li metal, NaOH pellets, or Zn acetate pellets with 18 MΩ water and 20%, 20%, and 10% glycerin by volume, respectively. The Whatman filters were dipped in solution until they were completely saturated. 37 mm Millipore AP10 cellulose support pads were prepared using the procedure outlined by Faivre-Pierret (1983). Each filter was impregnated with 1 ml of a1M Zn acetate – 10% glycerin solution. In all cases, the filters were allowed to air dry under a class 100 clean hood before being packed in plastic bags for transport. During sampling, the 47 mm filters were held in Nuclepore filter packs consisting of a 2 micron Zefluor Teflon filter (A) to trap aerosols, followed by two base-impregnated Whatman 41 cellulose filters (B and C). Samples were simultaneously collected on the Zn acetate-impregnated 37 mm Millipore pads. Two pads were held in a Millipore filter assembly. All joints were taped to prevent leaking. Following sampling, each filter pack was unloaded, and the filters were folded surface in to protect them. The filters were stored in sterile plastic Whirlpack bags and frozen until the time of analysis.

Radionuclide Counting

(^{210}Pb), (^{210}Bi), and (^{210}Po) activities were determined by counting the Poelmann-Schneider filters on α and β counters. β- decay of ^{210}Pb has two energies at 0.017 MeV and 0.061 MeV and ^{210}Bi has a β- decay of 1.162 MeV. β-emissions from ^{210}Bi are measured directly. Because the energies of ^{210}Pb are very low, after ^{210}Bi and ^{210}Pb are in equilibrium, β particles emitted from the decay of ^{210}Bi are measured as a proxy for

^{210}Pb. The beta counter was calibrated using a certified source of ^{40}K, which emits β particles with an energy of 1.3 MeV, very close to the energy of ^{210}Bi (Nho, 1996). ^{210}Po decays by α decay with an energy of 5.3044 MeV (Parrington et al., 1996). To calibrate the α counter, a radionuclide aerosol filter of known age was counted after ^{210}Po and ^{210}Pb have come into equilibrium. The ^{210}Pb activity is measured in the β counter, and the α counter is then calibrated by using ^{210}Pb to calculate the expected activity of ^{210}Po (P.-J. Gauthier, pers. comm.).

Beta counting on the 1999 filters was done immediately upon receipt of the filters at the Laboratoire des Sciences du Climat et de L'Environnement, Laboratoire Mixte CNRS/CEA between 22 December 1999 and 3 January 2000. The filters were analyzed in a single-sample beta counter with the entire sample surface exposed for counting. Samples were counted for 6 hours to give an initial indication of concentration and then continued up to 24 hours if activities were low. After complete decay of primary ^{210}Bi, the filters were recounted for β decays between 26 April 2000 and 2 May 2000 to measure the ^{210}Pb activity. Alpha decay of ^{210}Po was measured in a four-chamber alpha scintillation counter. The detector in each chamber measures emissions from only the inner half of each filter; therefore, every α decay measurement is doubled to account for decays on the outer portion of the filter. Each filter was counted for α decays for 24 hours in January 2000. Background activities are determined by a series of blank countings done before each set of samples. Corrections were made to account for decay during the time between sampling and counting using the equations in Appendix A.

Filters collected in 2000 and 2001 were counted by the same methods. Unfortunately, the 2001 samples arrived at the lab too late to make a β-counting for ^{210}Bi.

Ion Chromatography

The Zefluor and impregnated filters were analyzed by ion chromatography to determine sulfate concentrations. The 47 mm Zefluor and Whatman filters were cut in half using cleaned scissors, whereas the 37 mm filters were used whole. Each filter was leached in 18 g of 18 mΩ deionized water and 2 g of hydrogen peroxide in a 50 ml plastic centrifuge tube. The hydrogen peroxide ensured oxidization of any reduced sulfur species to sulfate. The tubes were shaken in a hot water bath for approximately 24 hours. Some of the Whatman filters completely dissolved into a pulp during the shaking process, whereas others remained intact. The LiOH-impregnated filters disintegrated entirely; the Zn acetate-impregnated filters broke up, but did not disintegrate; and the NaOH-impregnated filters remained mostly intact. In all cases, the 37 mm Millipore filters remained intact. The leached solutions were filtered through a 0.22 μm Millipore Express membrane into a second 50 ml plastic centrifuge tube. The filtering was necessary to avoid clogging the ion column during ion chromatography. Each solution was then transferred into a 20 ml glass scintillation vial for storage until analysis. Ion chromatography was performed at the New Mexico Bureau of Geology and Mineral Resources using a Dionex DX600 ion chromatograph with AS-14 column sets. The standard was a general lab standard made from Na_2SO_4. The Dionex IC automatically prepared dilutions of the standard to 1, 5, 10, 25, 50, and 100 ppm SO_4. The procedure used a carbonate/bicarbonate eluant and an analysis time of 20 minutes per sample. One sample of each type of impregnated filter was run as a duplicate to test reproducibility of the results.

Mineral Separates

A fresh lava bomb erupted on 10 December 2000 at 7:20 a.m. McMurdo local time was crushed and glass and minerals separated for ^{210}Po and ^{210}Pb analysis. 2 kg of crushed material ranging in size from <100 μm to approximately 1000 μm was split into four fractions. One fraction was ground to powder and then sieved through 100 μm nylon mesh. The remaining material larger than 100 μm was reground until the whole split was finer than 100 μm. Two fractions were sieved into several size ranges: >600 μm, 600 – 250 μm, 250 – 200 μm, 200 – 160 μm, 160 – 100 μm, and <100 μm. The three splits from 250 – 100 μm were washed to remove fine dust and then oven-dried. Each size range was separated into a glass separate, an anorthoclase separate, and a heavy mineral separate (olivine, pyroxene, and magnetite) using a Carpco electro-magnetic separator, a Frantz magnetic separator, and Bromoform heavy liquid.

Wet Chemistry and Alpha Spectroscopy

The emanation coefficient of Po was determined by measuring the amount of Po remaining in the magma after degassing as well as the amount in the volcanic gas plume. The emanation coefficient describes the partitioning of an element between the gas phase and the magma (Lambert et al., 1986). Po was extracted from the glass and whole rock separates. Approximately 3 grams of sample were mixed with a ^{209}Po spike so that the spike made up 10% of the final mass. Each sample was mixed with 10 ml hydrofluoric acid, 15 ml 8N hydrochloric acid, 3 ml perchloric acid and water and placed on a hot plate at 80°C. The hydrofluoric acid evaporated, while perchlorate remained in the solution, preventing fluorine deposition in the solution. The solution was heated

overnight to allow the sample to fully dissolve and then continued to evaporate for approximately one day. At this point, 5 ml hydrochloric acid and 5 ml boric acid were added to dissolve any remaining fluorides. This solution was heated to dryness on a hot plate overnight at 40°C and then redissolved in 50 ml 8N hydrochloric acid, 50 ml 5N hydrochloric acid, and a few drops of hydrogen peroxide. Once a new solution formed, ascorbic acid was added to reduce Fe^{2+} to Fe^{3+}, since Fe^{2+} interferes with deposition of Po onto silver. The Po deposited on a 16 mm diameter, 0.1 mm thick, plastic-backed, mirror-polished silver disk placed in the solution. ^{210}Po concentrations were measured using alpha spectrometry.

RESULTS

Samples

We collected aerosol samples for radionuclide analysis on Poelmann-Schneider blue cellulose filters. In 1999, 8 samples were collected over 10 days. Pump times varied from 43 to 139 minutes, with a pump rate of 20 m^3/hr (Table 1A). The volume of air sampled was in the 14 to 21 m^3 range apart from one sample which was collected for 139 minutes and had a sample volume of 46 m^3. In 2000, 20 samples were collected on 11 days spanning a 13 days period (10-22 December) (Table 1B). Pump times varied from 19 to 30 minutes, with pump rates varying from 5.6 to 9.2 m^3/hr. Sample volumes ranged from 1.4 to 4.2 m^3. In 2001, due to bad weather, only 4 samples were collected over 6 days (Table 1C). Pump times varied from 18 to 20 minutes, with a pump rate between 3 and 4.6 m^3/hr. Sample volumes ranged from 0.9 to 1.5 m^3.

In 1999, aerosols and acid gases were collected simultaneously with the radionuclides to determine the SO_2 concentration in the plume. Additional samples were taken at other times to measure the aerosol emissions (Table 2). Twenty-one 47 mm packs with Teflon and impregnated filters and ten 37 mm packs with Zn acetate impregnated filters were collected. Sample collection times varied from 31 to 289 minutes, with pump rates of ~18 L/min (1.1 m^3/hr). Blank samples were collected for all filter types by loading the filters into their holders and storing them for a few days before unloading and packing them for analysis. Aerosol and acid gas samples were also collected in 2000 and 2001; however, no data is available yet from these filters. The sample collection data for these years is presented in Appendix E.

Table 1A. Erebus radionuclide filters, December 1999

Sample	Date	Start Time[1]	Stop Time[1]	Total Time (min)	Volume (m^3)	Wind (knots)	Wind Dir	Plume Strength[2]	Sample
E99-15	10-Dec-99	1557	1700	63	21	7	S	1/10	E99-15
E99-18	11-Dec-99	1213	1315	62	21	2	S	5/10	E99-18
E99-21	11-Dec-99	2203	0022	139	46	0	nil	3/10	E99-21
E99-26	12-Dec-99	1051	1152	61	20	5	W	7/10	E99-26
E99-27	13-Dec-99	BLANK				n/a	n/a	n/a	E99-27
E99-30	13-Dec-99	1218	1301	43	14	2	W	4/10	E99-30
E99-31	13-Dec-99	1101	1201	60	20	2	W	4/10	E99-31
E99-36	14-Dec-99	1307	1409	62	21	0	nil	3/10	E99-36
E99-39	14-Dec-99	1421	1518	57	19	0	nil	5/10	E99-39

[1] All times McMurdo local summer time

[2] Plume strength indicates concentration of the plume on an empirical 1-10 scale with 10 being the most concentrated.

Pump rate = 20 m^3/hr (details in Appendix B)
n/a: no data due to BLANK filter

Table 1B. Erebus radionuclide filters, December 2000

Sample	Date	Start Time[1]	Stop Time[1]	Total Time (min)	Pump Start (cfm)	Pump End (cfm)	Pump Rate (m^3/hr)	Volume (m^3)	Wind (knots)	Wind Dir	Plume Strength[2]	Sample
E00-01	10-Dec-00	1437	1456	19	6.0	6.0	9.23	2.92	3	S	7/10	E00-01
E00-04	10-Dec-00	1500	1520	20	6.0	6.0	9.23	3.08	3	S	7/10	E00-04
E00-07	11-Dec-00	1042	1102	20	6.0	6.0	9.23	3.08	6	E,S	8/10	E00-07
E00-10	11-Dec-00	1106	1125	19	6.0	6.0	9.23	2.92	6	E,S	8/10	E00-10
E00-13	12-Dec-00	1239	1258	19	6.0	6.0	9.23	2.92	1	S	8/10	E00-13
E00-16	12-Dec-00	1633	1653	20	6.0	6.0	9.23	3.08	1	S	8/10	E00-16
E00-19	13-Dec-00	1530	1550	20	6.0	6.0	9.23	3.08	1	S,E	5/10	E00-19
E00-22	13-Dec-00	1555	1615	20	6.0	6.0	9.23	3.08	1	S,E	5/10	E00-22
E00-25	14-Dec-00	1319	1339	20	6.0	6.0	9.23	3.08	3	S	5/10	E00-25
E00-28	14-Dec-00	1342	1402	20	6.0	6.0	9.23	3.08	3	S	5/10	E00-28
E00-31	15-Dec-00	1243	1303	20	6.0	6.0	9.23	3.08	8	S	5/10	E00-31
E00-34	15-Dec-00	1309	1329	20	6.0	6.0	9.23	3.08	8	S	5/10	E00-34
E00-37	16-Dec-00	1354	1414	20	6.0	6.0	9.23	3.08	8	S	3/10	E00-37
E00-40	16-Dec-00	1422	1442	20	6.0	6.0	9.23	3.08	8	S	3/10	E00-40
E00-43	17-Dec-00	1556	1626	30	6.0	5.5	8.35	4.17	1	S	0/10	E00-43
E00-48	19-Dec-00	1222	1242	20	6.0	6.0	9.23	3.08	10	S	10/10	E00-48
E00-50	19-Dec-00	1246	1306	20	4.8	4.8	5.57	1.86	10	S	10/10	E00-50
E00-53	21-Dec-00	1728	1748	20	4.5	5.0	5.57	1.86	nd	nd	nd	E00-53
E00-55	21-Dec-00	1752	1812	20	4.8	4.8	5.57	1.86	nd	nd	nd	E00-55
E00-58	22-Dec-00	1712	1733	21	4.3	3.8	4.12	1.44	nd	nd	nd	E00-58
E00-67*	04-Jan-01	1318	1344	26	4.8	4.3	5.04	2.18	n/a	n/a	n/a	E00-67
E00-69*	04-Jan-01	1511	1612	61	4.3	4.5	4.79	4.87	n/a	n/a	n/a	E00-69

nd: no data recorded for these samples
*Samples E00-67 and E00-69 are background samples collected outside the plume.

Table 1C. Erebus radionuclide filters, December 2001

Sample	Date	Start Time[1]	Stop Time[1]	Total Time (min)	Pump Start (cfm)	Pump End (cfm)	Pump Rate (m^3/hr)	Volume (m^3)	Wind (knots)	Wind Dir	Plume Strength[2]	Sample
E01-01	08-Dec-01	1229	1248	19	4.5	4.1	4.65	1.5	15	S	7/10	E01-01
E01-04	11-Dec-01	1348	1407	19	3.8	3.5	3.54	1.1	2	S	2/10	E01-04
E01-06	11-Dec-01	1414	1432	18	3.5	3.0	3.04	0.9	2	S	2/10	E01-06
E01-09	13-Dec-01	1308	1328	20	4.8	2.5	3.54	1.2	>25	S	10/10	E01-09

Table 2. Erebus Sulfur Dioxide filters, December 1999

Sample	Date	A filt	B & C filters	Size (mm)	Start Time[1]	Stop Time[1]	Total Time (min)	Pump Start (scale)[2]	Pump Stop (scale)[2]	Flow Start (lpm)[3]	Flow Stop (lpm)[3]	Volume (liters)	Volume (m^3)	Wind (knots)	Wind Dir	Plume Strength[4]	Sample
E99-01	05-Dec-99	Z2.0	4Na	47	1319	1438	79	26	24	15	14	1162	1.16	0	nil	2/10	E99-01
E99-02	05-Dec-99	Z2.0	3Li	47	1319	1438	79	26	25	16	15	1194	1.19	0	nil	2/10	E99-02
E99-03	05-Dec-99	Z2.0	4Na	47	1443	1514	31	22	24	13	14	420	0.42	0	nil	2/10	E99-03
E99-04	05-Dec-99	Z2.0	3Li	47	1443	1514	31	20	25	11	15	403	0.40	0	nil	2/10	E99-04
E99-05	08-Dec-99	Z2.0	4Na	47	1459	1559	60	24	23	14	14	830	0.83	4	S	1/10	E99-05
E99-06	08-Dec-99	Z2.0	3Li	47	1455	1555	60	25	26	15	15	900	0.90	4	S	1/10	E99-06
E99-07	09-Dec-99	Z2.0	4Na	47	1634	1721	47	23	23	14	14	637	0.64	10	S	1/10	E99-07
E99-08	09-Dec-99	Z2.0	1Zn	47	1634	1721	47	26	26	16	16	746	0.75	10	S	1/10	E99-08
E99-09	09-Dec-99	Z2.0	4Na	47	BLANK									n/a	n/a	n/a	E99-09
E99-10	09-Dec-99	Z2.0	3Li	47	BLANK									n/a	n/a	n/a	E99-10
E99-11	09-Dec-99	Z2.0	1Zn	47	BLANK									n/a	n/a	n/a	E99-11
E99-12	10-Dec-99	Z2.0	1Zn	47	1600	1700	60	25	24	15	14	865	0.86	7	S	1/10	E99-12
E99-13	10-Dec-99		Zn Acetate	37	1600	1700	60	25	25	15	15	882	0.88	7	S	1/10	E99-13
E99-14	10-Dec-99		Zn Acetate	37	BLANK									n/a	n/a	n/a	E99-14
E99-16	11-Dec-99		Zn Acetate	37	1220	1320	60	26	26	16	15	935	0.93	2	S	5/10	E99-16
E99-17	11-Dec-99	Z2.0	1Zn	47	1220	1320	60	25	24	15	14	865	0.86	2	S	5/10	E99-17
E99-19	11-Dec-99		Zn Acetate	37	1328	1817	289	26	17	15	10	3608	3.61	2	S	5/10	E99-19
E99-20	11-Dec-99	Z2.0	3Li	47	1328	1817	289	24	17	14	10	3440	3.44	2	S	5/10	E99-20
E99-22	11-Dec-99		Zn Acetate	37	2203	0022	139	25	24	15	14	2004	2.00	0	nil	3/10	E99-22
E99-23	11-Dec-99	Z2.0	3Li	47	2203	0022	139	23	22	14	13	1844	1.84	0	nil	3/10	E99-23
E99-24	12-Dec-99		Zn Acetate	37	1056	1156	60	26	26	16	15	935	0.93	5	W	7/10	E99-24
E99-25	12-Dec-99	Z2.0	3Li	47	1056	1156	60	23	26	14	15	865	0.87	5	W	7/10	E99-25
E99-28	13-Dec-99		Zn Acetate	37	1208	1300	52	26	25	15	15	780	0.78	2	W	4/10	E99-28
E99-29	13-Dec-99	Z2.0	1Zn	47	1208	1300	52	26	26	15	16	810	0.81	2	W	4/10	E99-29
E99-32	13-Dec-99	Z2.0	3Li	47	1103	1203	60	22	26	13	15	848	0.85	2	W	4/10	E99-32
E99-33	13-Dec-99		Zn Acetate	37	1103	1203	60	26	26	15	15	917	0.92	2	W	4/10	E99-33
E99-34	14-Dec-99	Z2.0	3Li	47	1309	1409	60	22	26	13	15	848	0.85	0	nil	3/10	E99-34
E99-35	14-Dec-99		Zn Acetate	37	1309	1409	60	26	26	15	15	917	0.92	0	nil	3/10	E99-35
E99-37	14-Dec-99	Z2.0	1Zn	47	1414	1514	60	26	26	15	15	917	0.92	0	nil	5/10	E99-37
E99-38	14-Dec-99		Zn Acetate	37	1414	1514	60	26	26	15	15	917	0.92	0	nil	5/10	E99-38
E99-40	15-Dec-99	Z2.0	4Na	47	BLANK									n/a	n/a	n/a	E99-40

Z2.0: Zefluor Teflon filter, 2 micron pore size ; 4Na: 4M NaOH prepared 19 Nov 1999; 3Li: 3M LiOH prepared 16 Nov 1999; 1Zn: 1M Zn acetate prepared 18 Nov 1999
37 mm Zn acetate filters prepared by M.-F. LeCloarec, Gif-sur-Yvette, France.
[2]Scaled flow corrected for Erebus barometric pressure and temperature using HI-Q Environmental Tables A-31031 and A-32422 (Appendix B).
[3]Liters/minute calculated from flowmeter scale using Gilmont Instruments flowmeter calibration data (Appendix B).
[4]Plume strength indicates concentration of the plume on a 1-10 scale with 10 being the most concentrated.
n/a: no data due to BLANK filter

Radionuclides

Radionuclide concentrations varied widely on the 8 filters collected in 1999 (Table 3A; Appendix C). Blank values on the filters are zero for ^{210}Bi and ^{210}Po and 3 disintegrations per thousand seconds (mBq) for ^{210}Pb. Analytical uncertainties are based on counting statistics and are ~ 0.5% for ^{210}Po, 1% for ^{210}Bi and 2% for ^{210}Pb at the 1σ level. Raw counting data are given in Appendix C.

Within the samples the (^{210}Po) has the highest and (^{210}Pb) the lowest activities. Blank-corrected initial activities, indicated by a $^{\circ}$ superscript, were corrected back to the time of collection on the crater rim. The (^{210}Po)$^{\circ}$ ranges from 316 to 55,716 mBq; (^{210}Pb)$^{\circ}$ from 0 to 978 mBq; and (^{210}Bi)$^{\circ}$ from 185 to 18,232 mBq (Table 3) excluding sample E99-27 which was a blank. The highest activities were seen on sample E99-26 and were collected on a day when the plume was blowing over the pump site and was also at its greatest strength (Table 1).

The concentration of radionuclide species in the volcanic plume is a valuable measurement that is useful for comparing these species with others such as SO_2. To allow a comparison, activities are expressed in terms of the activities per volume of air sampled during pumping (Table 3). As previously noted, most filters sampled between 14 to 19 m^3 of air. Concentrations of (^{210}Pb)$^{\circ}$, (^{210}Bi)$^{\circ}$, and (^{210}Po)$^{\circ}$ range from 3 to 48 mBq/m^3, 4 to 904 mBq/m^3, and 7 to 2762 mBq/m^3, respectively. A plume that is mixed with a large amount of air will yield very low concentrations of radionuclides, as these species are not found in ambient air. Samples collected outside of the plume show little or no radionuclide activity.

Table 3A. Blank corrected initial activities (in mBq) and concentrations (in mBq/m^3) for ^{210}Pb, ^{210}Bi and ^{210}Po and calculated activity ratios in filters collected at Mount Erebus in 1999. Activities are indicated by the brackets and have been corrected to the collection time of the samples and indicated by ( )$^\circ$

Sample	Volume (m^3)	(^{210}Pb)$^\circ$ (mBq)	(^{210}Bi)$^\circ$ (mBq)	(^{210}Po)$^\circ$ (mBq)	(^{210}Pb)$^\circ$ (mBq/m^3)	(^{210}Bi)$^\circ$ (mBq/m^3)	(^{210}Po)$^\circ$ (mBq/m^3)	(Po/Pb)$^\circ$	(Bi/Pb)$^\circ$
E99-15	21	190	3364	13561	**9**	**161**	**651**	**71**	**18**
E99-18	21	253	4853	15600	**12**	**237**	**761**	**62**	**19**
E99-21	46	0	185	316	**0**	**4**	**7**	**0**	**0**
E99-26	20	978	18232	55716	**48**	**904**	**2762**	**57**	**19**
E99-27	Blank	0	0	0	**0**	**0**	**0**	**0**	**0**
E99-30	14	133	3185	12455	**9**	**224**	**876**	**94**	**24**
E99-31	20	344	7192	16709	**17**	**363**	**842**	**49**	**21**
E99-36	21	52	641	5627	**3**	**31**	**274**	**109**	**12**
E99-39	19	279	2750	19179	**15**	**146**	**1018**	**69**	**10**

Although the absolute concentration of radionuclide species sampled will vary with the concentration of the plume, the activities ratios of species should remain constant, despite plume dilution. Thus, radionuclide activities are reported in terms of the activity ratios $(^{210}Po/^{210}Pb)^{\circ}$ and $(^{210}Bi/^{210}Pb)^{\circ}$. Activity ratios for $(^{210}Po/^{210}Pb)^{\circ}$ range from 49 to 109, with a mean and standard deviation of 58±37. $(^{210}Bi/^{210}Pb)^{\circ}$ range from 10 to 24, with a mean and standard deviation of 18±9 (Table 3A). Figure 2 shows the positive correlation of $(^{210}Pb)^{\circ}$ versus $(^{210}Po)^{\circ}$ and $(^{210}Bi)^{\circ}$.

As in 1999, in 2000 the initial radionuclide activities varied widely on filters (Table 3B). The activities are lower than those seen in 1999 due to a lower pumping rate and shorter sampling time. In 2000, no absolute blanks were counted for background; however, two samples, E00-67 and E00-68, were collected at the Lower Erebus Hut to measure background counts in the atmosphere outside of the direct influence of the plume. On these filters, (^{210}Po) and (^{210}Bi) are zero. There is a significant ^{210}Pb blank of 5 mBq. ^{210}Po activities are highest, while ^{210}Pb activities are lowest for all filters. The range for blank-corrected initial activities of $(^{210}Po)^{\circ}$ is 150 to 10,058 mBq; for $(^{210}Pb)^{\circ}$ the range is 3 to 133 mBq; and for $(^{210}Bi)^{\circ}$ the range is 0 to 2275 mBq. The one very low sample, E00-43, was collected during a period of very calm winds when little plume blew over the pumping site. The concentration of ^{210}Po ranges from 36 to 3665 mBq/m^3; ^{210}Pb concentration ranges from 1 to 72 mBq/m^3; and ^{210}Bi concentration ranges from 0 to 1706 mBq/m^3. The activity ratio for $(^{210}Po/^{210}Pb)^{\circ}$ ranges from 39 to 92, with a mean and standard deviation of 68±12. The activity ratio for $(^{210}Bi/^{210}Pb)^{\circ}$ ranges from 0 to 29, with a mean and standard deviation of 19±6.

In 2001, four samples were collected, with $(^{210}Po)^{o}$ activities ranging from 267 to 6967 mBq and $(^{210}Pb)^{o}$ activities ranging from 6 to 157 mBq. The concentration of ^{210}Po ranges from 161 to 3011 mBq/m^3; ^{210}Pb concentration ranges from 4 to 68 mBq/m^3. The activity ratio for $(^{210}Po/^{210}Pb)^{o}$ varies from 44 to 62, with a mean and standard deviation of 47 ± 9. The samples with the highest and lowest activity ratios were collected minutes apart on the same day.

Table 3B. Blank-corrected initial activities and concentrations for ^{210}Pb, ^{210}Bi and ^{210}Po and calculated activity ratios in filters collected at Mt Erebus in 2000.

Sample	Volume (m^3)	(210Pb)° (mBq)	(210Bi)° (mBq)	(210Po)° (mBq)	(210Pb)° mBq/m^3	(210Bi)° mBq/m^3	(210Po)° mBq/m^3	(Bi/Pb)°	(Po/Pb)°
E 00-01	2.92	86	1451	5572	29	496	1906	17	65
E 00-04	3.08	75	1457	4675	24	473	1519	19	62
E 00-07	3.08	115	2143	8773	37	696	2850	19	76
E 00-10	2.92	128	2275	10058	44	778	3440	18	78
E 00-13	2.92	91	1739	7369	31	595	2520	19	81
E 00-16	3.08	24	246	1430	8	80	465	10	60
E 00-19	3.08	16	64	634	5	21	206	4	39
E 00-22	3.08	27	322	1893	9	105	615	12	70
E 00-25	3.08	67	1128	4111	22	366	1336	17	61
E 00-28	3.08	106	2016	6816	34	655	2214	19	65
E 00-31	3.08	56	964	3110	18	313	1010	17	56
E 00-34	3.08	32	480	1892	11	156	615	15	58
E 00-37	3.08	82	1422	4856	27	462	1578	17	59
E 00-40	3.08	75	1393	4408	24	453	1432	19	59
E 00-43	4.17	3	0	150	1	0	36	0	44
E 00-48	3.08	100	1928	6924	33	626	2250	19	69
E 00-50	1.86	97	1865	6808	52	1004	3665	19	70
E 00-53	1.86	133	3169	8557	72	1706	4607	24	64
E 00-55	1.86	70	1138	4149	38	613	2234	16	59
E 00-58	1.44	8	231	738	6	160	513	29	92
E 00-67	2.18	0	0	1	0	0	1	n/a	n/a
E 00-69	4.87	0	0	0	0	0	0	n/a	n/a

Table 3C. Initial activities and concentrations for ^{210}Pb and ^{210}Po and the calculated activity ratio in filters collected at Mt Erebus in 2001.

Sample	Volume (m3)	(210Pb)° (mBq)	(210Po)° (mBq)	**(210Pb)° (mBq/m3)**	**(210Po)° (mBq/m3)**	**(Po/Pb)°**
E01-01	2.31	157	6967	**68**	**3011**	**44**
E01-04	1.95	43	2650	**22**	**1359**	**62**
E01-06	1.66	6	267	**4**	**161**	**44**
E01-09	2.05	124	6033	**60**	**2939**	**49**

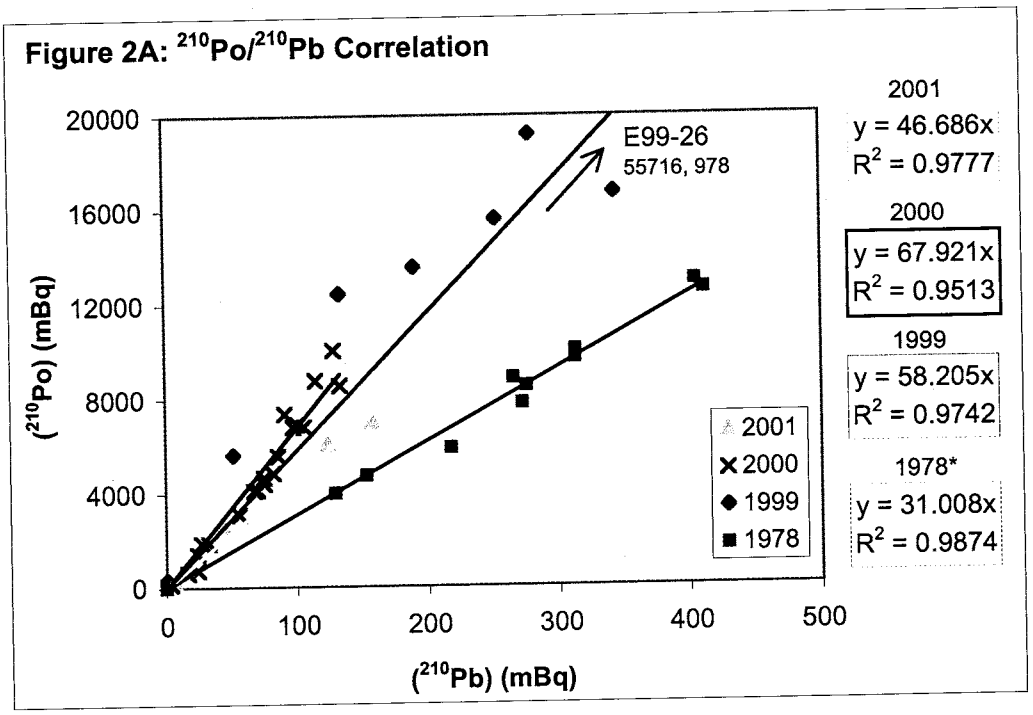

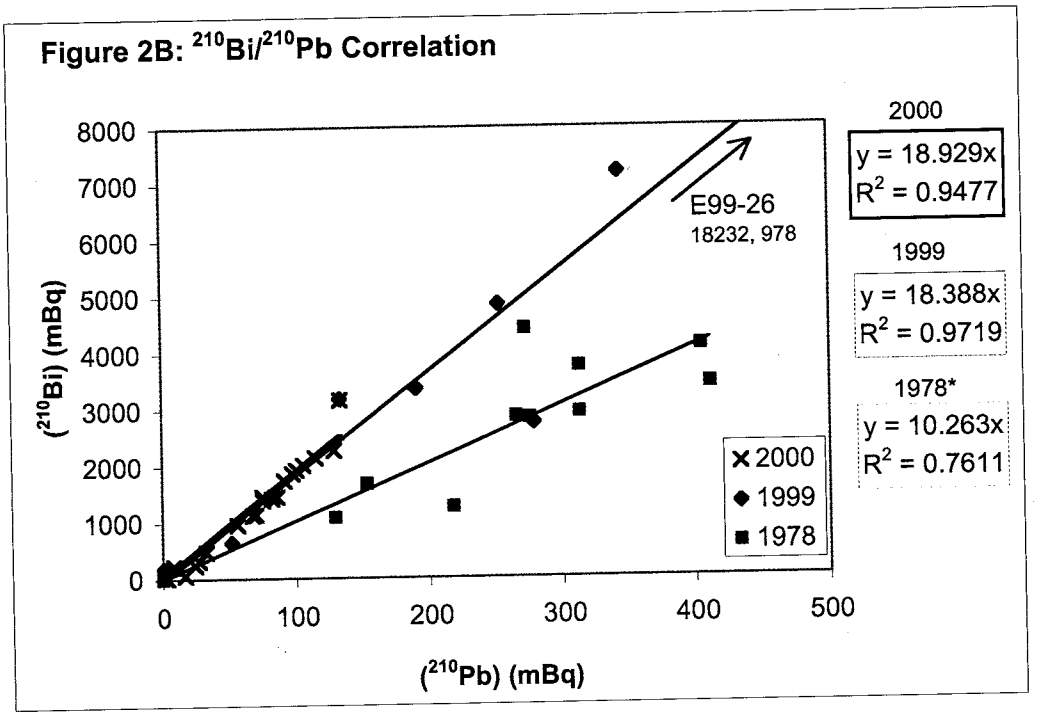

Figure 2. (^{210}Pb) is plotted against (^{210}Po) (2A) and (^{210}Bi) (2B) for the Mount Erebus plume. Calculated best fit lines for the two species are shown and are a function of plume dilution with ambient air. A sample that plots near the origin is very dilute, while a high, outlying 1999 sample (E99-26) is from a very concentrated plume. This sample is plotted off the chart. Average ($^{210}Po/^{210}Pb$) and ($^{210}Bi/^{210}Pb$) are given by the slopes of the mixing lines. *Polian and Lambert, 1979.

Sulfur

Sulfur concentrations were measured on the impregnated filters for samples collected in 1999, but not 2000 or 2001. Like the radionuclides, these concentrations vary widely, once again due to dilution of the plume at the time of sampling (Table 4). The ion chromatography analyses are reported as ppm SO_4 in the dissolved filter solution. These mixing ratios are converted into values of μg S collected in each filter pack and μg S/m^3 of air sampled. Raw sulfur data is presented in Appendix D. Sample volumes are mostly in the range of 0.40 m^3 to 1.2 m^3, with pump times on the order of 1 hour. Samples E99-19 and E99-20 were pumped for 289 minutes and consequently have very high sample volumes of 3.61 m^3 and 3.44 m^3, respectively. Samples E99-22 and E22-23 were pumped for 139 minutes and have volumes of 2.00 and 1.84 m^3. NaOH-impregnated filters have concentrations ranging from 58 – 945 μg S/m^3 air. The NaOH filters give very erratic results, with individual blank values higher than values on sampled filters. Because of the erratic and high blank values, these values will not be used in final calculations. The results from the Zn acetate-impregnated and LiOH-impregnated filters were somewhat better than the NaOH filters. For LiOH filters, concentrations ranged from 31 – 927 μg S/m^3 air. Concentrations on 47 mm Zn acetate filters ranged from 72 – 420 μg S/m^3 air, while concentrations on 37 mm Zn acetate filters ranged from 28 – 838 μg S/m^3 air. The blank values used are 0.30 ppm for the Zefluor filters, 0.51 for the LiOH filters, 0.505 for the 47 mm Zn acetate filters, and 0.905 for the 37 mm Zn acetate filters. Analytical errors on the SO_4 measurements are in the range of 6-12%, based on duplicate analysis of several samples.

For each radionuclide sampling interval, S was collected on two filter packs of different types. The highest S concentration of 927 μg S/m^3 was seen on sample E99-25, a LiOH filter collected simultaneously with E99-24, a 37 mm filter with a concentration of 687 μg S/m^3. Sample E99-16 has a concentration of 838 μg S/m^3, the highest concentration seen on the 37 mm filters. This filter was collected simultaneously with a 47 mm Zn acetate pack, sample E99-17, which has a concentration of 420 μg S/m^3. E99-17 shows the highest concentration of this filter type.

An average ratio of ^{210}Pb to S in the plume can be found by comparing the measured concentrations of each species. Figure 3 shows the correlation between S and ^{210}Pb concentrations for those sampling periods when both species were collected. The 37 mm S sample E99-16 was discarded due to an erratic concentration. While the 37 mm filters give the most consistent S values, the concentrations are much lower on these filters than on 47 mm filters collected simultaneously. It is probable that not all the S was fully extracted during the leaching process. To bring the concentrations on the 37 mm filters in line with 47 mm measurements, all concentrations were multiplied by a correction factor of 1.59. This correction results in ^{210}Pb/S ratio in the plume of 0.05 mBq/m^3 for both 37 mm and 47 mm filters.

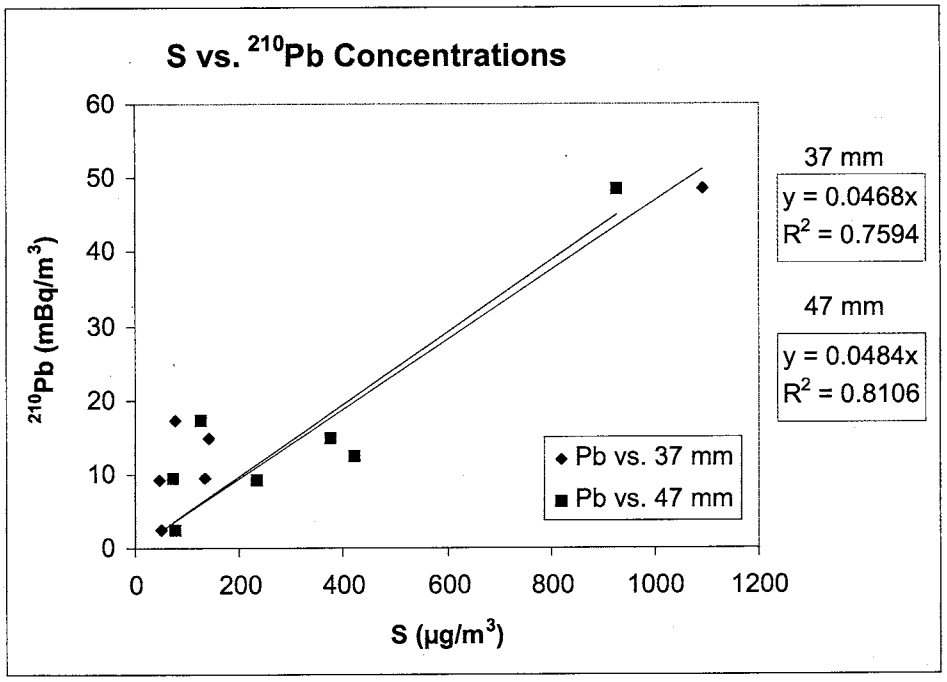

Figure 3. Correlation of ^{210}Pb versus S concentration in the Mount Erebus plume in 1999 using corrected 37 mm data.

Table 4. Erebus SO_2 filters collected in December 1999, grouped by sampling time. Uncorrected S concentration in the plume at the time of sampling is shown on the right.

Sample	Date	A filt	B & C filters	Size (mm)	Start Time	Stop Time	Total Time (min)	Volume (m^3)	$\mu g\ S/m^3$ air
E99-01	05-Dec-99	Z2.0	4Na	47	1319	1438	79	1.16	57.5
E99-02	05-Dec-99	Z2.0	3Li	47	1319	1438	79	1.19	24.5
E99-03	05-Dec-99	Z2.0	4Na	47	1443	1514	31	0.42	279.2
E99-04	05-Dec-99	Z2.0	3Li	47	1443	1514	31	0.40	207.0
E99-05	08-Dec-99	Z2.0	4Na	47	1459	1559	60	0.83	944.7
E99-06	08-Dec-99	Z2.0	3Li	47	1455	1555	60	0.90	134.6
E99-07	09-Dec-99	Z2.0	4Na	47	1634	1721	47	0.64	428.5
E99-08	09-Dec-99	Z2.0	1Zn	47	1634	1721	47	0.75	214.5
E99-09	09-Dec-99	Z2.0	4Na	47	BLANK				
E99-10	09-Dec-99	Z2.0	3Li	47	BLANK				
E99-11	09-Dec-99	Z2.0	1Zn	47	BLANK				
E99-13	10-Dec-99		1Zn	37	1600	1700	60	0.88	27.8
E99-12	10-Dec-99	Z2.0	1Zn	47	1600	1700	60	0.86	232.5
E99-14	10-Dec-99		1Zn	37	BLANK				
E99-16	11-Dec-99		1Zn	37	1220	1320	60	0.93	838.4
E99-17	11-Dec-99	Z2.0	1Zn	47	1220	1320	60	0.86	420.4
E99-19	11-Dec-99		1Zn	37	1328	1817	289	3.61	263.7
E99-20	11-Dec-99	Z2.0	3Li	47	1328	1817	289	3.44	531.5
E99-22	11-Dec-99		1Zn	37	2203	0022	139	2.00	84.5
E99-23	11-Dec-99	Z2.0	3Li	47	2203	0022	139	1.84	371.4
E99-24	12-Dec-99		1Zn	37	1056	1156	60	0.93	686.6
E99-25	12-Dec-99	Z2.0	3Li	47	1056	1156	60	0.87	926.7
E99-28	13-Dec-99		1Zn	37	1208	1300	52	0.78	84.0
E99-29	13-Dec-99	Z2.0	1Zn	47	1208	1300	52	0.81	71.6
E99-33	13-Dec-99		1Zn	37	1103	1203	60	0.92	48.9
E99-32	13-Dec-99	Z2.0	3Li	47	1103	1203	60	0.85	126.8
E99-35	14-Dec-99		1Zn	37	1309	1409	60	0.92	31.7
E99-34	14-Dec-99	Z2.0	3Li	47	1309	1409	60	0.85	76.2
E99-38	14-Dec-99		1Zn	37	1414	1514	60	0.92	90.1
E99-37	14-Dec-99	Z2.0	1Zn	47	1414	1514	60	0.92	374.7
E99-40	15-Dec-99	Z2.0	4Na	47	BLANK				

DISCUSSION

Calculation of Parameters

Several parameters describe the partitioning of elements between different phases in the magmatic system. The partition coefficient, D, is the distribution of an element X between the gas and liquid (melt) phases, and is given by

$$D_X = [X]_G/[X]_L,$$

where $[X]_G$ is the concentration of X in the gas phase and $[X]_L$ is the concentration of X in the liquid (melt). The amount of gas species X that escapes or is emitted is given by the emanation coefficient ε_X (Gill et al., 1985; see also Lambert et al., 1986 and Le Cloarec and Lambert, 1993). The emanation coefficient is given by

$$\varepsilon_X = N_G/N_0,$$

where N_G is the number of atoms of the species in the gas phase and N_0 is the number of atoms of the species in the magma prior to degassing. D_X and ε_X are related to the pre-eruptive volatile content, α, by:

$$\varepsilon_X = \frac{\alpha D_X}{\alpha D_X + 1 - \alpha}.$$

A full treatment of the relationship between the partition coefficient and the emanation coefficient is given in Appendix A in Gauthier et al. (2000).

The emanation coefficient for a species must be estimated, and then the distribution coefficient can be calculated. The ε_{Po} for the Erebus magma is 0.45, based on alpha spectrometry of glass and whole rock splits (P.-J. Gauthier, pers. comm.). Assuming that the parental material is a deep magma of basanitic composition, the pre-eruptive volatile content of the magma is ~2.5% (Eschenbacher, 1998). Using an

emanation coefficient for Po $\varepsilon_{Po} = 0.45$, the partition coefficient $D_{Po} = 31.74$ for a basanitic composition, with 2.5% volatiles. If the parental magma has a more evolved tephriphonolite with a pre-eruptive volatile content of 0.63% (Eschenbacher, 1998), the $D_{Po} = 129$.

The ε_{Pb} is normally calculated by comparing ^{210}Pb and S concentrations in the plume to $^{210}Pb/S$ in the undegassed magma. Since ^{226}Ra in not volatile at magmatic temperatures, the ^{226}Ra activity in the lava can be used as a proxy for ^{210}Pb activity in the deep magma in radioactive equilibrium. Comparing the ^{226}Ra activity of 0.08667 Bq/g (K. Sims, pers. comm.) to Eschenbacher's (1998) measurement of 2166 ppm S in olivine-hosted melt inclusions in basanitic lavas (sample DVDP 3-295), the atomic ratio of $^{210}Pb/S$ in the undegassed magma is 2.16×10^{-12}. Sulfur and ^{210}Pb concentrations in the plume are available from filters collected simultaneously during the 1999 field season. The average ratio of $^{210}Pb/S$ is 0.05 mBq/g S, giving an atomic ratio of 2.7×10^{-12}. These numbers indicate that ^{210}Pb is slightly more volatile than S. These findings correlate with those of Symonds et al. (1990) for Augustine volcano and Symonds et al. (1987) for Merapi volcano. Pb and S have similar enrichment factors at both volcanoes, with Pb enrichment being slightly higher or lower than that of S based on the sampling location (dome, fumarole, etc.) and sample type (condensate, sublimate, etc.) The S concentration in the matrix glass of Eschenbacher's sample DVDP 3-295 is 505 ppm, indicating that 77% of the original S was degassed, giving an $\varepsilon_{Pb} = 0.96$. In most basaltic systems, ε_{Pb} falls between 0.01 – 0.015 (Lambert et al., 1986; Pennisi and Le Cloarec, 1998). $\varepsilon_{Pb} = 0.96$ is an unrealistically high value. A likely explanations is that the magma had already exsolved S before the melt inclusions were trapped. It is also possible that the basanite is

not the most representative material for estimating the degassing of the Erebus phonolite. Without an accurate pre-eruptive S concentration, ε_{Pb} cannot be calculated using this method. An alternative is to calculate ε_{Pb} from the ratio of $(^{210}Pb)_L/(^{210}Pb)_0$. Gamma counting of a whole rock split gives a ^{210}Pb activity in the lava of 0.085 Bq/g (P.-J. Gauthier, pers. comm.). A comparison of ^{210}Pb activity in the degassed lava to Sims' measurement of ^{226}Ra = 0.08667 Bq/g in the magma (the non-volatile ^{226}Ra can be used as a proxy for ^{210}Pb in the undegassed system in radioactive equilibrium) shows that over 98% of ^{210}Pb remains in the magma after degassing. However, ε_{Pb} = 0.019 can be viewed only as a maximum value due to possible loss of some atoms during ^{222}Rn degassing. If ^{222}Rn atoms are lost from the system, the ^{210}Pb activity in the lava is lower than expected, giving a higher emanation coefficient. It is realistic to assume a Pb emanation coefficient in the range of 0.01 to 0.015, which is a typical range for basaltic magmas (Rubin, 1997). In the degassing model, the $(^{210}Po/^{210}Pb)$ ratio must fall between $\varepsilon_{Po}/\varepsilon_{Pb}$ for a highly renewed magma chamber and D_{Po}/D_{Pb} for a poorly renewed chamber (Gauthier, et al., 2000). The ratio of emanation coefficients is the lower limit for the $(^{210}Po/^{210}Pb)$ ratio because if the radionuclides are in equilibrium in the shallow magma (as is the case in a system that has a very short residence time), then $\varepsilon_{Po}/\varepsilon_{Pb}$ represents the radionuclide activity ratio in the gas phase. If the activities of two species N_1 and N_2 are equal, then $\lambda_1N_1 = \lambda_2N_2$ and $\lambda_1N_1/\lambda_2N_2 = 1$. By multiplying each activity by the emanation coefficient for that species, ε_1 and ε_2, the expression becomes $\varepsilon_1\lambda_1N_1/\varepsilon_2\lambda_2N_2$, which reduces to $\varepsilon_1/\varepsilon_2$. Using this expression with the ratios from each year gives a range for ε_{Pb} of 0.007 – 0.01. A value of ε_{Pb} = 0.01 overlaps both with this range and with the typical range for basaltic magmas and gives a partition coefficient D_{Pb} = 0.39 with a

basanite parent and 1.59 with a tephriphonolite parent. This method of determining the emanation coefficient involves some circular reasoning, in that the emanation coefficient is chosen partly to fit the data instead of being independently determined; however a lead emanation coefficient of 0.01 is a reasonable value for a general basaltic system and for Erebus specifically. Using a higher or lower value would create a situation in which the degassing model does not work for ratios from all years, implying that the emanation coefficient changes from year to year. This would indicate a change in magma chemistry, which is unlikely at Erebus.

The range for the Bi emanation coefficient is estimated using the same premise of the degassing model that ($^{210}Bi/^{210}Pb$) falls between $\varepsilon_{Bi}/\varepsilon_{Pb}$ and D_{Bi}/D_{Pb}. The recharge rate model equation is not very sensitive to the D_{Bi} value; the calculated residence time varies by less than 1% over the range of D_{Bi}, so an estimation of the value does not have a strong effect on the final calculated values. The Bi emanation coefficient falls in a range from 0.16 to 0.19, giving D_{Bi} ranging from 7.3 – 8.8 for a basanite parent or 30 – 37 for a tephriphonolite parent.

A possible source of error for the partition coefficients is the calculation of pre-eruptive volatile content. In the basanite lava, pre-eruptive volatiles are ~2.5%. However, Eschenbacher (1998) believes that CO_2 could be degassing from a source much deeper than the ~4.5 km depth of these melt inclusion samples. Therefore, the pre-eruptive volatile content of the degassing magma as estimated from melt inclusions can only be considered a minimum value. The pre-eruptive volatile content has a large effect on the partition coefficient, but Gauthier et al. (2000) show that a large change in D

changes the activity ratios in the model by a factor that is not greater than analytical uncertainty.

Calculation of Magma Recharge Rate

Gauthier et al. (2000) developed a degassing model that was used to estimate magma recharge rates and residence times at Stromboli volcano using measured ($^{210}Po/^{210}Pb$) and ($^{210}Bi/^{210}Pb$). This model should be usable to estimate these parameters at other volcanoes that experience steady-state activity. Using Equation 12 from Gauthier et al. (2000) with known parameters from Mount Erebus, it should be possible to determine the recharge rate and residence times of the degassing magma in the system.

Activity ratios for $^{210}Po/^{210}Pb$ are available for 1999, 2000, and 2001. For all years, when assuming a basanite parent with $\alpha = 2.5\%$, then $D_{Pb} = 0.39$, $D_{Bi} = 8.8$, and $D_{Po} = 31.74$. Graphing the model equation with these parameters creates a curve to calculate recharge rates or residence times for changing ($^{210}Po/^{210}Pb$) (Figure 4). The equation may also be solved directly, using activity ratios measured each year. In 1999, ($^{210}Po/^{210}Pb$) = 58.2, giving a modeled recharge rate of 0.005 d^{-1},or 1.8 y^{-1}, and a residence time, τ, of 203 days. The residence time is the reciprocal of the recharge rate per unit time. In 2000, ($^{210}Po/^{210}Pb$) = 67.9, giving a modeled recharge rate of 0.002 d^{-1}, or 0.6 y^{-1}, and a residence time of 606 days. In 2001, ($^{210}Po/^{210}Pb$) dropped to 46.686. This drop corresponds to an increase in recharge rate to 0.06 d^{-1}, or 21 y^{-1}, and a decrease in residence time to 17 days. Table 5 summarizes the activity ratios and parameters for each year. If the parental material is a tephriphonolite with $\alpha = 0.63\%$, then $D_{Pb} = 1.59$, $D_{Bi} = 36$, and $D_{Po} = 129$. These changes in the values of the partition coefficients do not

cause a large change in the calculated values of recharge rate and residence time of degassing magma. In 1999, the recharge rate is 0.004 d^{-1}, or 1.5 y^{-1}, corresponding to a residence time of 215 days. In 2000, the recharge rate drops to 0.0014 d^{-1}, or 0.5 y^{-1}, and the residence time rises to 648 days. In 2001, the recharge rate increases to 0.5 d^{-1} or 18 y^{-1}, with a residence time of 20 days.

Table 5. Parameters (α, D) and activity ratios used in the degassing model to calculate recharge rates (ϕ_0/M) and residence times (τ) for each year.

Year	(^{210}Po/^{210}Pb)	(^{210}Bi/^{210}Pb)	α (%)	D_{Pb}	D_{Bi}	D_{Po}	ϕ_0/M (year^{-1})	τ (day)
1999	58.2	18.4	2.5	0.39	8.8	31.7	1.8	203
			0.63	1.59	36	129	1.5	215
2000	67.9	18.9	2.5	0.39	8.8	31.7	0.6	606
			0.63	1.59	36	129	0.5	648
2001	46.7	n/a	2.5	0.39	8.8	31.7	21	17
			0.63	1.59	36	129	18	20

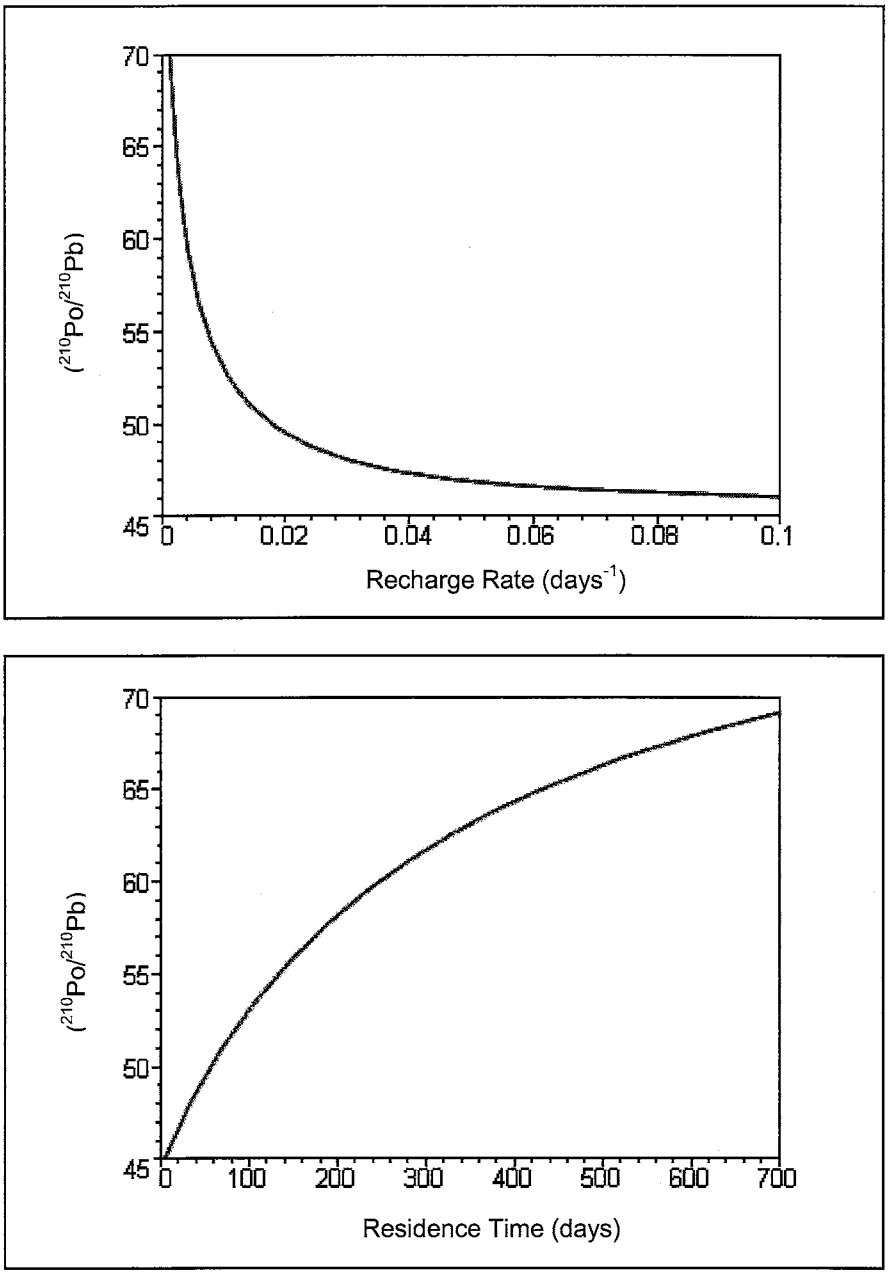

Figure 4. Graphs of recharge rates (top) and residence times (bottom) for changing 210Po/210Pb activity ratios in the Erebus magma using the degassing model equation.

These results indicate that a long period of low renewal in 1999 and 2000 was followed by a period of much higher recharge in 2001. Klimasauskas (1995) proposed that the magma chamber is heterogeneous and experiences large-scale convection. It is

possible that the changing activity ratios demonstrate this convection occurs as batches of magma at different stages of disequilibrium degas at the surface. However, if the degassing magma has a constant composition, these residence time calculations tell us an interesting story about the dynamics of the magma chamber.

Deep Magma Recharge

From October 2000 to July 2001, volcanic tremor evidenced magma movement at a depth of 5-7 km (Ruiz et al., 2002). In January 2001 lava flowed out of an auxiliary vent located west of the main lava lake, indicating a rise in the level of the underlying magma.. A small amount of tilt (~0.1 mm/d) was also observed during this time (Kyle et al., 2002). These events all point toward a recharge of new magma into the system over the course of 2000 and into early 2001. According to the model presented in Gauthier et al. (2000), an influx of new, undegassed magma to the upper part of the system will result in lower values of (^{210}Po/^{210}Pb) and (^{210}Bi/^{210}Pb). The undegassed magma is in radioactive equilibrium, and all activity ratios are equal to 1. The gas from this magma will have a (^{210}Po/^{210}Pb) activity ratio close to 45, based on the ratio of the emanation coefficients of these species. The addition of this magma to partially degassed magma will bring the observed ratios in the gas plume closer to 45 as well. However, at Erebus, (^{210}Po/^{210}Pb) and (^{210}Bi/^{210}Pb) are elevated in the 2000 samples. According to the model, this increase indicates that the recharge at this time was lower than normal. All other physical evidence points to a deep recharge event occurring before and during the 2000 sampling period.

One explanation of the observed changes in ($^{210}Po/^{210}Pb$) seen from 1999 to 2001 is that, while physical evidence may show a deep recharge event, that magma was too deep to be degassing during the 2000 field season. The deep magma could push the existing magma up higher in the chamber, causing the lava flows seen early in 2001. Over the course of 2001, this new magma would rise and mix with the degassing magma in the shallow part of the system. At this point, the magma would degas, giving a recharge signature of a lower ($^{210}Po/^{210}Pb$), which is what we see in 2001 when this value drops from 68 to 46 over the year. This timescale is consistent with Klimasauskas' (1985) conclusions that the system experiences a cyclic overturn on the order of 2 – 3 years.

Degassing Magma Volume

Knowing the magma residence time, τ, should allow us to calculate a volume for the degassing magma. The residence time is the inverse of the recharge rate per unit time; therefore, $M=\phi_0 \times \tau$. The volume, $V=M/\rho$. Harris et al. (1999) used Landsat thematic mapper data to estimate a mass flux at Erebus of 30-76 kg/s. The average density of the Erebus magma is 2700 kg/m^3 (Dunbar et al., 1994). Using these values for mass flux and density and the calculated residence times (using the assumption of a basanite parent), the volume of degassing magma in 1999 has a possible range of 1.9 – 4.9×10^5 m^3, the volume in 2000 has a range of 5.8 – 14.7×10^5 m^3; and the volume in 2001 has a range of 0.16 – 0.41×10^5 m^3. These values imply that the volume, and consequently mass, of the magma in the degassing system are changing dramatically from one year to the next. If this is the case, it negates the assumption of steady state that

is necessary to use the degassing model. A more likely situation is that the mass flux changes over time, while the volume remains relatively constant. Rearranging the equations for volume calculation gives $\phi_0=V\times\rho/\tau$, showing that to maintain a constant volume, the mass flux varies inversely with the residence time. During 1999 and 2000, as the residence time increased, the flux of new magma was fairly low. In 2001, the decrease in residence time indicates a much larger mass flux, which is in agreement with the theory of injection of new material affecting the degassing system during late 2001.

ENVIRONMENTAL CONSIDERATIONS

In addition to their applications in determining magma chamber dynamics and processes, U-series daughters, especially ^{210}Po and ^{210}Pb, are effective tracers of volcanic plume dispersal (Arimoto et al., 2001; Nho et al., 1997; Su and Huh, 2002). Nho et al. (1997) measured ^{210}Po near the Indonesian arc and determined that air with admixed volcanic plume (as opposed to air with normal continental origins containing ^{210}Po from the decay of ^{222}Rn soil gas) contains significantly higher levels of ^{210}Po (up to 66 $\mu Bq/m^3$, as compared with 5 $\mu Bq/m^3$ for continental air). Even though ^{222}Rn decay and volcanic gas contribute equal amounts of ^{210}Po to the global budget, the ^{210}Po magnitude is much higher in air derived from a volcanic point source (Nho et al., 1997). It is likely that, due to low soil exposure on Antarctica, the bulk of ^{210}Po in the Antarctic atmosphere is volcanic. Also, while ^{210}Po is highly susceptible to washout (Nho et al., 1997), low aridity and absence of ice crystals in Antarctica makes this factor negligible (Tabazadeh and Turco, 1993). Therefore, ^{210}Po measured at the South Pole is likely to be highly representative of Erebus ^{210}Po emissions. From December 1998 through January 1999

and December 2000 - January 2001, Arimoto et al. (2001; 2002) measured ^{210}Po and ^{210}Pb aerosols at the South Pole as part of the Investigation of Sulfur Chemistry in the Antarctic Troposphere (ISCAT) Program. Their objective was to determine the influence of non-sea salt sulfate on the Antarctic sulfur budget. They observed (^{210}Po/^{210}Pb) activity ratios in the range of 0.13 – 0.18 over the two field seasons (Arimoto et al., 2002 submitted).

Other estimates of Mount Erebus' contribution to the Antarctic vary widely. Using a simple rectangular box model, Zreda-Gostynska et al. (1997) estimated that sulfur from Erebus accounts for ~3% of total atmospheric sulfur in Antarctica. Using an atmospheric dispersion model, Klimasauskas (1995) estimated that Erebus sulfur could account for ~10 – 100% of sulfur at the South Pole. Zreda-Gostynska et al. (1997) also analyzed Pb isotopic ratios in Erebus lava to show that Antarctic snow is highly contaminated with Erebus-derived Pb, refuting the conclusions of Rosman et al. (1994) that much of the Pb in the Antarctic snow has an anthropogenic source. Wardell et al. (2002) also provide evidence that Pb flux from Erebus is enough to account for the Pb measured in South Pole snow. Using ^{210}Po as a tracer of the Erebus plume, it may be possible to make more accurate estimates of Erebus' contribution to the levels of S, F, Cl and many metals in the Antarctic environment.

We can estimate the percentage of sulfate that Erebus contributes to the South Pole by comparing S and ^{210}Po measurements made at both locations. Over the two field seasons of the ISCAT Program, the average $SO_4^{2-}/^{210}$Po ratio was 247×10^6 g/pCi (R. Arimoto, pers. comm.). The average ^{210}Po/S ratio measured at Erebus is 2.8×10^3 Bq/g (Figure 5), which is equivalent to 39.6×10^6 g/pCi. Assuming that 100% of the ^{210}Po at

the South Pole originates in the Erebus plume, comparing these numbers shows that Erebus contributes ~16% of the sulfate measured at the South Pole.

We can use a similar approach to estimate the volcano's contribution of Pb to the South Pole atmosphere. ($^{210}Po/^{210}Pb$) activity ratios at Mount Erebus range from 47 – 68 during 1999, 2000 and 2001. ($^{210}Po/^{210}Pb$) activity ratios at the South Pole were 0.18 during the 1998-1999 ISCAT field season and 0.13 during the 2000-2001 season (Arimoto et al., 2002 submitted). Comparing the two ratios indicates that 0.2% of the ^{210}Pb at the South Pole originates at Mount Erebus. At most, ^{210}Pb from Erebus could make up 0.4% of the total ^{210}Pb at the South Pole. We would expect a strong Erebus influence to manifest as a ^{210}Po enrichment compared to ^{210}Pb, as Lambert et al. (1979) saw at Dumont-d'Urville (67°S, Antarctic coast, Terre Adelie) in samples with ($^{210}Po/^{210}Pb$) ranging from 2.7 – 7.4. Clearly, a significant part of the ^{210}Pb at the South Pole has another atmospheric source. The average ($^{210}Po/^{210}Pb$) ratio in the troposphere as a result of radon flux from soils is ~0.5 (Polian and Lambert, 1979). ^{222}Rn has a global flux of 3×10^9 Ci/y, which decays to 1.5×10^6 Ci/y ^{210}Pb, and finally to 6×10^4 Ci/y ^{210}Po (Lambert et al., 1966). Residence times in the troposphere are too short to allow these species to come into radioactive equilibrium, and ^{210}Po decay is assumed to be minimal during transport from Erebus to South Pole. Over the southern hemisphere, the ($^{210}Po/^{210}Pb$) ratio in the stratosphere is close to 1 (Sanak et al., 1978). The very low ratios measured at the South Pole indicate a ^{210}Pb source other than normal atmospheric mixing. It is possible that this is an anthropogenic lead source, supporting the findings of Rosman et al. (1994). However, since our measurements are only of ^{210}Pb, there could be

a much larger relative flux of other Pb isotopes coming from Erebus. In order to use these data definitively, we would need to measure the ^{210}Pb/Pb ratio in the Erebus plume.

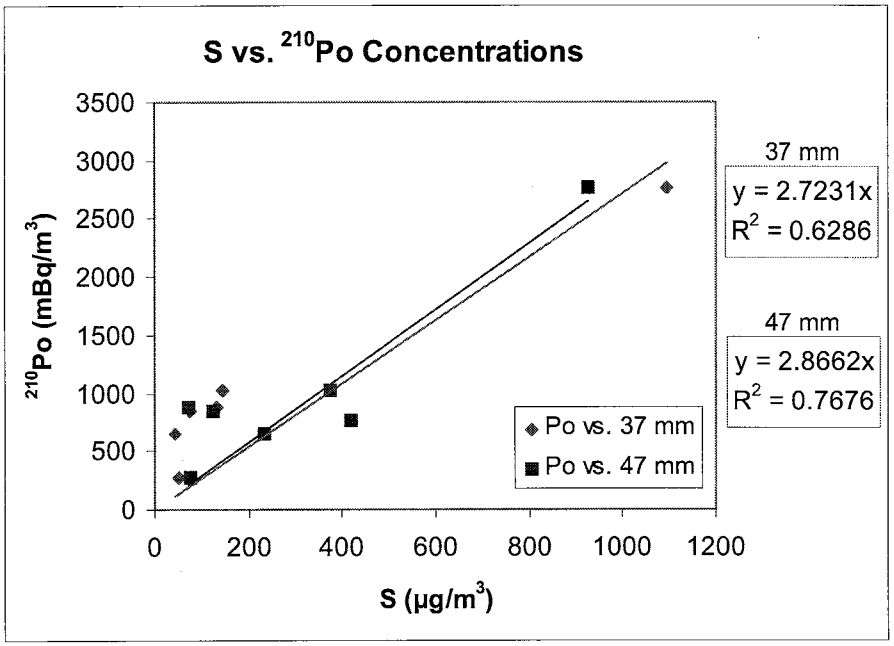

Figure 5. Correlation of ^{210}Po versus S concentration in the Mount Erebus plume in 1999.

CONCLUSIONS

Geochemical models are a powerful tool to assess the physical nature of a magma chamber. Past research (Gauthier and Condomines, 1999; Lambert et al., 1986; Le Cloarec and Lambert, 1993) shows that changes in volatile uranium daughters can be used to monitor the dynamics of a shallow magma body. Using a degassing model developed by Gauthier et al. (2000), we have calculated the residence time and volume of the degassing material in the Mount Erebus magmatic system using measured activity ratios of the ^{238}U decay chain radionuclides ^{210}Pb, ^{210}Bi, and ^{210}Po.

Samples collected during three field seasons show distinct changes affecting the degassing magma body. From 1999 to 2000, residence times increased as influx of new magma slowed. In 2001, the residence time dramatically decreased, signaling that a pulse of fresh magma was degassing.

The model of Gauthier et al. (2000) proposes using residence time in conjunction with a constant mass flux to calculate a volume of degassing magma; however, the large variation in residence time at Erebus from one year to the next creates unrealistic volume changes. A more realistic model involves residence time changing as a result of variable mass flux. At Erebus, we observed a lower mass flux in 1999 and 2000 followed by a sharp increase in 2001.

The evidence of influx of new material to the shallow part of the magma chamber in late 2001 could be the result of deep magma movement during the preceding year, evidenced by volcanic tremor and slight deformation of the volcano during 2000 and early 2001. In agreement with Klimasauskas' (1985) conclusions, this timing points toward large-scale cycling in the magma chamber on the order of 2 – 3 year.

Due to low soil exposure and precipitation in the Antarctic, it is likely that most of the ^{210}Po measured at the South Pole originates at Mount Erebus, making ^{210}Po an effective tracer of the Erebus plume. By comparing $^{210}Po/S$ and ($^{210}Po/^{210}Pb$) ratios in both the plume and the South Polar atmosphere, we estimate that Erebus is the source of ~16 – 28% of the SO_4^{2-} and ~0.2 – 0.4% of the ^{210}Pb measured at the South Pole. These results indicate that there is a very large source of Pb in the Antarctic atmosphere other than Mount Erebus.

REFERENCES

Andres, R.J. and Kasgnoc, A.D., 1998. A time-averaged inventory of subaerial volcanic sulfur emissions. Journal of Geophysical Research, 103: 25251-25261.

Arimoto, R., Hogan, A., Webb, J., Grube, P., Davis, D., Schloesslin, C., Sage, S., 2002 submitted. Major ions, trace elements, and radionuclides in aerosol particles from the South Pole during ISCAT-2000. Geophysical Research Letters.

Arimoto, R., Nottingham, A.S., Webb, J. and Schloesslin, C.A., 2001. Non-sea salt sulfate and other aerosol constituents at the South Pole during ISCAT. Geophysical Research Letters, 28(19): 3645-3648.

Caldwell, D.A. and Kyle, P.R., 1994. Mineralogy and geochemistry of ejecta erupted from Mount Erebus, Antarctica, between 1972 and 1986. In: P.R. Kyle (Editor), Volcanological and Environmental Studies of Mount Erebus, Antarctica. Antarctic Research Series. American Geophysical Union, Washington, D.C., pp. 147-162.

Chouet, B.A., 1996. Long-period volcano seismicity: its source and use in eruption forecasting. Nature, 380: 309-316.

Condomines, M., Hemond, C. and Allegre, C.J., 1988. U-Th-Ra radioactive disequilibria and magmatic processes. Earth and Planetary Science Letters, 90: 243-262.

Cooper, A.K., Davey, F.J. and Behrendt, J.C., 1987. Seismic stratigraphy and structure of the Victoria Land Basin, western Ross Sea, Antarctica. In: A.K. Cooper and F.J. Davey (Editors), The Antarctic continental margin; geology and geophysics of the western Ross Sea. Circum-Pacific Council for Energy and Mineral Resources, Earth Science Series, Houston, TX, pp. 27-76.

Dibble, R.R., 1994. Velocity modeling in the erupting magma column of Mount Erebus, Antarctica. In: P.R. Kyle (Editor), Volcanological and Environmental Studies of Mount Erebus, Antarctica. Antarctic Research Series. American Geophysical Union, Washington, D.C., pp. 1-16.

Dibble, R.R., Barrett, S.I.D., Kaminuma, K., Miura, S., Kienle, J., Rowe, C., Kyle, P.R., and McIntosh W.C., 1988. Time comparisons between video and seismic signals from explosions in the lava lake of Erebus volcano, Antarctica. Bulletin of the Disaster Prevention Research Institute, 38: 147-161.

Dunbar, N.W., Cashman, K.V. and Dupre, R., 1994. Crystallization processes of anorthoclase phenocrysts in the Mount Erebus magmatic system: evidence from crystal composition, crystal size distributions, and volatile contents of melt inclusions, Volcanological and Environmental Studies of Mount Erebus, Antarctica. Antarctic Research Series. American Geophysical Union, Washington, D.C., pp. 129-146.

Eschenbacher, A., 1998. Open-system degassing of a fractionating, alkaline magma, Mount Erebus, Ross Island, Antarctica. M.S. Thesis, New Mexico Institute of Mining and Technology, Socorro, NM, 89 pp.

Esser, R.P., Kyle, P.R. and McIntosh, W.C., submitted. $^{40}Ar/^{39}Ar$ dating of the eruptive history of Mount Erebus, Antarctica: volcano evolution. Bulletin of Volcanology.

Faivre-Pierret, R., 1983. SO_2, HCl, and HF detection and dosing in the volcanic gas phase. In: H. Tazieff and J.-C. Sabroux (Editors), Forecasting Volcanic Events. Elsevier, New York, pp. 399-408.

Garces, M.A., Hagerty, M.T. and Schwartz, S.Y., 1998. Magma acoustics and time-varying melt properties at Arenal volcano, Costa Rica. Geophysical Research Letters, 25(13): 2293-2296.

Gauthier, P.-J. and Condomines, M., 1999. ^{210}Pb-^{226}Ra radioactive disequilibria in recent lavas and radon degassing: inferences on the magma chamber dynamics at Stromboli and Merapi volcanoes. Earth and Planetary Science Letters, 172: 111-126.

Gauthier, P.-J., Le Cloarec, M.-F. and Condomines, M., 2000. Degassing processes at Stromboli volcano inferred from short-lived disequilibria (^{210}Pb-^{210}Bi-^{210}Po) in volcanic gases. Journal of Volcanology and Geothermal Research, 102: 1-19.

Giggenbach, W.F., Kyle, P.R. and Lyon, G.L., 1973. Present volcanic activity on Mount Erebus, Ross Island, Antarctica. Geology, 1: 135-136.

Gill, J.B., Williams, R.W. and Bruland, K., 1985. Eruption of basalt and andesite lava degases 222Rn and 210Po. Geophysical Research Letters, 12(1): 17-20.

Hagerty, M.T., Schwartz, S.Y., Protti, M., Garces, M.A. and Dixon, T., 1997. Observations at Costa Rican volcano offer clues to causes of eruptions. EOS, Transactions of the American Geophysical Union, 78(49): 565-571.

Harris, A.J.L., Flynn, L.P., Rothery, D.A., Oppenheimer, C. and Sherman, S.B., 1999. Mass flux measurements at active lava lakes: Implications for magma recycling. Journal of Geophysical Research, 104(B4): 7117-7136.

Ivanovich, M., 1992. The phenomenon of radioactivity. In: M. Ivanovich and R.S. Harmon (Editors), Uranium-series Disequilibrium. Oxford University Press, New York, pp. 1-33.

Kaminuma, K., 1994. The seismic activity of Mount Erebus in 1981-1990. In: P.R. Kyle (Editor), Volcanological and Environmental Studies of Mount Erebus, Antarctica. Antarctic Research Series. American Geophysical Union, Washington, D.C., pp. 1-16.

Klimasauskas, E.P., 1995. Emission and dispersion of gaseous S, F, Cl from Mt. Erebus, Antarctica. M.S. Thesis, New Mexico Institute of Mining and Technology, Socorro, New Mexico, 95 pp.

Kyle, P.R., 1977. Mineralogy and glass chemistry of recent volcanic ejecta from Mt. Erebus, Ross Island, Antarctica. New Zealand Journal of Geology and Geophysics, 20: 1123-1146.

Kyle, P.R., 1990. McMurdo Volcanic Group, Western Ross Embayment: Introduction. In: W.E. LeMasurier and J.W. Thomson (Editors), Volcanoes of the Antarctic

Plate and Southern Ocean. American Geophysical Union, Washington, D.C., pp. 19-25.

Kyle, P.R. and Cole, J.W., 1974. Structural control of volcanism in the McMurdo Volcanic Group, Antarctica. Bulletin of Volcanology, 38: 16-25.

Kyle P.R., Desmarais E., Meertens C., Kurnik C., Johns B., and McIntosh W.C., 2002 In search of volcanic deformation at Mount Erebus, Antarctica. Poster, UNAVCO Annual Meeting, 26-28 February 2002, Colorado Springs, CO.

Kyle, P.R., Moore, J.A. and Thirlwall, M.F., 1992. Petrologic evolution of anorthoclase phonolite lavas at Mount Erebus, Ross Island, Antarctica. Journal of Petrology, 33(4): 849-875.

Kyle, P.R., Sybeldon, L.M., McIntosh, W.C., Meeker, K. and Symonds, R., 1994. Sulfur dioxide emission rates from Mount Erebus, Antarctica. In: P.R. Kyle (Editor), Volcanological and Environmental Studies of Mount Erebus, Antarctica. Antarctic Research Series. American Geophysical Union, Washington, D.C., pp. 69-82.

Lambert, G., Ardouin, B., Nezami, M. and Polian, G., 1966. Possibilities of using lead 210 as an atmospheric tracer. Tellus, 18: 421-426.

Lambert, G., Buisson, A., Sanak, J. and Ardouin, B., 1979. Modification of the atmospheric polonium 210 to lead 210 ratio by volcanic emissions. Journal of Geophysical Research, 84(C11): 6980-6986.

Lambert, G., Le Cloarec, M.F., Ardouin, B. and Le Roulley, J.C., 1986. Volcanic emission of radionuclides and magma dynamics. Earth and Planetary Science Letters, 76: 185-192.

Le Cloarec, M.F. and Lambert, G., 1993. Volcanic radionuclides: A tool for estimating magma reservoirs. Trends in Geophysical Research, 2: 173-181.

Le Cloarec, M.F., Lambert, G., Le Roulley, J.C. and Ardouin, B., 1986. Long-lived radon decay products in Mount St. Helens emissions: An estimation of the magma reservoir volume. Journal of Volcanology and Geothermal Research, 28: 85-89.

Nho, E.-Y., 1996. Le polonium 210 dans les aerosols: contribution a l'etude des feux de savanes et des emissions volcaniques. Ph.D. Thesis, Universite Paris VII, Paris.

Nho, E.-Y., Le Cloarec, M.-F., Ardouin, B. and Ramonet, M., 1997. ^{210}Po, an atmospheric tracer of long-range transport of volcanic plumes. Tellus, 49B: 429-438.

Parrington, J.R., Knox, H.D., Breneman, S.L., Baum, E.M. and Feiner, F., 1996. Nuclides and Isotopes. General Electric Co. and KAPL, Inc.

Pennisi, M. and Le Cloarec, M.-F., 1998. Variations of Cl, F, and S in Mount Etna's plume, Italy, between 1992 and 1995. Journal of Geophysical Research, 103(B3): 5061-5066.

Polian, G. and Lambert, G., 1979. Radon daughters and sulfur output from Erebus Volcano, Antarctica. Journal of Volcanology and Geothermal Research, 6: 125-137.

Pyle, D.M., 1992. The volume and residence time of magma beneath active volcanoes determined by decay-series disequilibria methods. Earth and Planetary Science Letters, 112: 61-73.

Rose, W.I., Chuan, R.L. and Kyle, P.R., 1985. Rate of sulphur dioxide emission from Erebus volcano, Antarctica, December 1983. Nature, 316(6030): 710-712.

Rosman, K.J.R., Chisholm, W., Boutron, C.F., Candelone, J.-P. and Patterson, C.C., 1994. Anthropogenic lead isotopes in Antarctica. Geophysical Research Letters, 21: 2669-2672.

Rowe, C.A., Aster, R.C., Kyle, P.R., Dibble, R.R. and Schlue, J.W., 2000. Seismic and acoustic observations at Mount Erebus Volcano, Ross Island, Antarctica, 1994-1998. Journal of Volcanology and Geothermal Research, 101: 105-128.

Rubin, K., 1997. Degassing of metals and metalloids from erupting seamount and mid-ocean ridge volcanoes: observations and predictions. Geochimica et Cosmochimica Acta, 61: 3525-3542.

Ruiz, M.C., Aster, R.C., Kyle, P.R. and Mah, S., 2002. Recent tremor activity on Mount Erebus, Antarctica. 2002 Meeting of the Seismological Society of America, 17-19 April 2002, Victoria, BC.

Sanak, J., Lambert, G. and Ardouin, B., 1978. Lead-210 in the atmosphere. In: F. Gesell and W.M. Lowder (Editors), Natural Radiation Environment 3. National Technical Information Service, U.S. Department of Commerce, pp. 445-457.

Su, C.-C. and Huh, C.-A., 2002. Atmospheric 210Po anomaly as a precursor of volcano eruptions. Geophysical Research Letters, 29(5): 14-1-14-4.

Symonds, R.B., Rose, W.I., Gerlach, T.M., Briggs, P.H. and Harmon, R.S., 1990. Evaluation of gases, condensates, and SO_2 emissions from Augustine volcano, Alaska: the degassing of a Cl-rich volcanic system. Bulletin of Volcanology, 52: 355-374.

Symonds, R.B., Rose, W.I., Reed, M.H., Lichte, F.E. and Finnegan, D.L., 1987. Volatization, transport and sublimation of metallic and non-metallic elements in high temperature gases at Merapi Volcano, Indonesia. Geochimica et Cosmochimica Acta, 51: 2083-2101.

Tabazadeh, A. and Turco, R.P., 1993. Stratospheric chlorine injection by volcanic eruptions: HCl scavenging and implications for ozone. Science, 260: 1082-1086.

Volpe, A.M. and Hammond, P.E., 1991. ^{238}U-^{230}Th-^{222}Ra disequilibria in young Mount St. Helens rocks: time constraint for magma formation and crystallization. Earth and Planetary Science Letters, 107: 475-486.

Wardell, L.J., Kyle, P.R. and Counce, D., submitted. Volcanic emissions of metals and halogens from White Island, New Zealand and Mt. Erebus, Antarctica determined

using chemical traps, Geophysical Monograph, Volcanism and the Earth's Atmosphere. American Geophysical Union, Washington, DC.

Williams, R.W. and Gill, J.B., 1989. Effects of partial melting on the uranium decay series. Geochimica et Cosmochimica Acta, 53: 1607-1619.

Williams, R.W., Gill, J.B. and Bruland, K.W., 1986. Ra-Th disequilibria systematics: Timescale of carbonatite magma formation at Oldoinyo Lengai volcano, Tanzania. Geochimica et Cosmochimica Acta, 50: 1249-1259.

Zreda-Gostynska, G., Kyle, P.R., Finnegan, D. and Prestbo, K.M., 1997. Volcanic gas emissions from Mount Erebus and their impact on the Antarctic environment. Journal of Geophysical Research, 102(B7): 15039-15055.

APPENDIX A: Derivation of radioactive decay equations used to calculate initial activities of ^{210}Pb-^{210}Bi-^{210}Po based on radioactive counting completed days or weeks after sampling (M.-F. LeCloarec, pers. comm.).

^{210}Pb	→	^{210}Bi	→	^{210}Po	→	^{206}Pb
1	22.4 y	2	5.02 d	3	138.3 d	

Initial concentrations, number of atoms present:
N_{01} N_{02} N_{03}

^{210}Pb:

$$\boxed{N_1(t) = N_{01}e^{-\lambda_1 t}}$$

^{210}Bi:

(1) $\frac{dN_1}{dt} = -N_1\lambda_1$ describes the decay of ^{210}Pb → ^{210}Bi

(2) $\frac{dN_2}{dt} = N_1\lambda_1 - N_2\lambda_2 = \lambda_1 N_{01}e^{-\lambda_1 t} - N_2\lambda_2$

describes both the decay of ^{210}Pb → ^{210}Bi and ^{210}Bi → ^{210}Po

General Form of the decay equation for the second member of a decay chain; solve for coefficients A and B:

(3) $N_2 = Ae^{-\lambda_1 t} + Be^{-\lambda_2 t}$

(4) $\frac{dN_2}{dt} = -A\lambda_1 e^{-\lambda_1 t} - B\lambda_2 e^{-\lambda_2 t}$ derivative of (3)

at time t = 0:

(5) $N_2 = N_{02} = A + B$ from (3)

(6) $\frac{dN_2}{dt} = \lambda_1 N_{01} - \lambda_2 N_{02} = -A\lambda_1 - B\lambda_2$ from (2) and (4)

System of 2 equations with 2 unknowns:

(7) $A = N_{02} - B$ from (5)

(8) $\lambda_1 N_{01} - \lambda_2 N_{02} = -\lambda_1(N_{02} - B) - B\lambda_2$ substituting (7) into (6)

$\lambda_1 B - \lambda_2 B - \lambda_1 N_{02} = \lambda_1 N_{01} - \lambda_2 N_{02}$

$B(\lambda_1 - \lambda_2) = \lambda_1 N_{01} + N_{02}(\lambda_1 - \lambda_2)$

$$B = \frac{\lambda_1 N_{01}}{\lambda_1 - \lambda_2} + N_{02}$$

$$A = \frac{-\lambda_1 N_{01}}{\lambda_1 - \lambda_2}$$

(9) $$\boxed{N_2(t) = \frac{\lambda_1 N_{01}}{\lambda_2 - \lambda_1} e^{-\lambda_1 t} + \left[N_{02} - \frac{\lambda_1 N_{01}}{\lambda_2 - \lambda_1} \right] e^{-\lambda_2 t}}$$

substituting solutions for A and B into (3)

$$\lambda_2 N_2 = \frac{\lambda_1 \lambda_2 N_{01}}{\lambda_2 - \lambda_1} e^{-\lambda_1 t} + \lambda_2 N_{02} e^{-\lambda_2 t} - \frac{\lambda_1 \lambda_2 N_{01}}{\lambda_2 - \lambda_1} e^{-\lambda_2 t}$$ multiplying (9) by λ_2

(10) $$= \frac{\lambda_1 \lambda_2 N_{01}}{\lambda_2 - \lambda_1} (e^{-\lambda_1 t} - e^{-\lambda_2 t}) + \lambda_2 N_{02} e^{-\lambda_2 t}$$ and simplifying

^{210}Po:

(11) $$\frac{dN_3}{dt} = \lambda_2 N_2 - \lambda_3 N_3$$

describing decay from ^{210}Bi → ^{210}Po and from ^{210}Po → its daughter

(12) $$\frac{dN_3}{dt} = \frac{\lambda_1 \lambda_2 N_{01}}{\lambda_2 - \lambda_1} (e^{-\lambda_1 t} - e^{-\lambda_2 t}) + \lambda_2 N_{02} e^{-\lambda_2 t} - \lambda_3 N_3$$

substituting (10) into (11)

General Form of the decay equation for the third member of the decay chain; solve for coefficients A, B and C:

(13) $$N_3 = Ae^{-\lambda_1 t} + Be^{-\lambda_2 t} + Ce^{-\lambda_3 t}$$

at time t = 0:

(14) $$N_3 = N_{03} = A + B + C$$ from (13)

(15) $$\frac{dN_3}{dt} = -A\lambda_1 - B\lambda_2 - C\lambda_3 = \lambda_2 N_{02} - \lambda_3 N_{03}$$

derivative of (13) at t=0 set equal to (11)

(16) $$\frac{dN_3}{dt} = -A\lambda_1 e^{-\lambda_1 t} - B\lambda_2 e^{-\lambda_2 t} - C\lambda_3 e^{-\lambda_3 t}$$ derivative of (13)

introduce $\lambda_3 N_3 - \lambda_3 N_3$ as a zero term into (16), substituting (13) in for the first N_3

(17) $$\frac{dN_3}{dt} = \lambda_3 (Ae^{-\lambda_1 t} + Be^{-\lambda_2 t} + Ce^{-\lambda_3 t}) - \lambda_3 N_3 - A\lambda_1 e^{-\lambda_1 t} - B\lambda_2 e^{-\lambda_2 t} - C\lambda_3 e^{-\lambda_3 t}$$

(18) $$= A(\lambda_3 - \lambda_1) e^{-\lambda_1 t} + B(\lambda_3 - \lambda_2) e^{-\lambda_2 t} - \lambda_3 N_3$$

simplifying (17)

Solving for the $e^{-\lambda_1 t}$ coefficient from (13):

(19) $$A(\lambda_3 - \lambda_1) = \frac{\lambda_1 \lambda_2 N_{01}}{\lambda_2 - \lambda_1}$$

$$(20)\quad A = \frac{\lambda_1\lambda_2 N_{01}}{(\lambda_2-\lambda_1)(\lambda_3-\lambda_1)}$$

Solving for the $e^{-\lambda_2 t}$ coefficient from (13):

$$(21)\quad B(\lambda_3-\lambda_2) = \lambda_2 N_{02} - \frac{\lambda_1\lambda_2 N_{01}}{\lambda_2-\lambda_1}$$

using the $e^{-\lambda_2 t}$ coefficients from (12) and (18)

$$(22)\quad B = \frac{\lambda_2 N_{02}}{\lambda_3-\lambda_2} - \frac{\lambda_1\lambda_2 N_{01}}{(\lambda_3-\lambda_2)(\lambda_2-\lambda_1)}$$

Solving for C from (13):

$$C = N_{03} - A - B$$

$$= N_{03} - \frac{\lambda_1\lambda_2 N_{01}}{(\lambda_2-\lambda_1)(\lambda_3-\lambda_2)} - \frac{\lambda_2 N_{02}}{\lambda_3-\lambda_2} + \frac{\lambda_1\lambda_2 N_{01}}{(\lambda_3-\lambda_2)(\lambda_2-\lambda_1)}$$

substituting (20) and (22) for A and B

$$= N_{03} - \frac{\lambda_2 N_{02}}{\lambda_3-\lambda_2} + \frac{\lambda_1\lambda_2 N_{01}}{\lambda_2-\lambda_1}\left[\frac{1}{(\lambda_3-\lambda_2)} - \frac{1}{(\lambda_3-\lambda_1)}\right]$$

$$= N_{03} - \frac{\lambda_2 N_{02}}{\lambda_3-\lambda_2} + \frac{\lambda_1\lambda_2 N_{01}}{\lambda_2-\lambda_1}\left[\frac{\lambda_3-\lambda_1-\lambda_3+\lambda_2}{(\lambda_3-\lambda_2)(\lambda_3-\lambda_1)}\right]$$

$$C = N_{03} - \frac{\lambda_2 N_{02}}{\lambda_3-\lambda_2} + \frac{\lambda_1\lambda_2 N_{01}}{(\lambda_3-\lambda_2)(\lambda_3-\lambda_1)}$$

$$N_3(t) = \frac{\lambda_1\lambda_2 N_{01}}{(\lambda_3-\lambda_1)(\lambda_2-\lambda_1)}e^{-\lambda_1 t} + \frac{\lambda_2}{\lambda_3-\lambda_1}\left(N_{02} - \frac{\lambda_1 N_{01}}{\lambda_2-\lambda_1}\right)e^{-\lambda_2 t} + \left[N_{03} - \frac{\lambda_2}{\lambda_3-\lambda_2}\left(N_{02} - \frac{\lambda_1 N_{01}}{\lambda_3-\lambda_1}\right)\right]e^{-\lambda_3 t}$$

APPENDIX B: Pump Calibration and Corrections for Pressure and Temperature

Gast Regenair R1102 Pump Calibration

The flow rate on the Gast Regenair pump, used for radionuclide sampling in 1999, was measured in the lab in Socorro, New Mexico using an anemometer to measure air speed across a cellulose filter.

Filter area, $A = 0.0029 m^2$
Average air velocity, $V = 1.9$ m/s = 6840 m/hr
Flow rate, $Q = V \times A = 19.84\ m^3/hr$

The velocity of the air flow on Mount Erebus would change due to slight changes in the viscosity of the air sampled; however, this effect would be negligible compared to other errors associated with sampling and flow measurement.

HI-Q CF-18V Pump Calibration

The HI-Q CF-18V pump has a built-in calibrated flow meter that measures air flow in CFM. The air velocity across a filter was measured in the field using an anemometer to make an accurate conversion from CFM to m^3/hr. Conversions use a filter diameter of 0.06 m, giving $m^3/hr = m/s \times 3600\ s/hr \times (0.03m)^2 \times \pi$.

CFM	m/s	m^3/hr
3.0	0.28	2.8
3.5	0.33	3.4
4.0	0.38	3.9
4.5	0.49	5.0
5.0	0.62	6.3
5.5	0.75	7.6

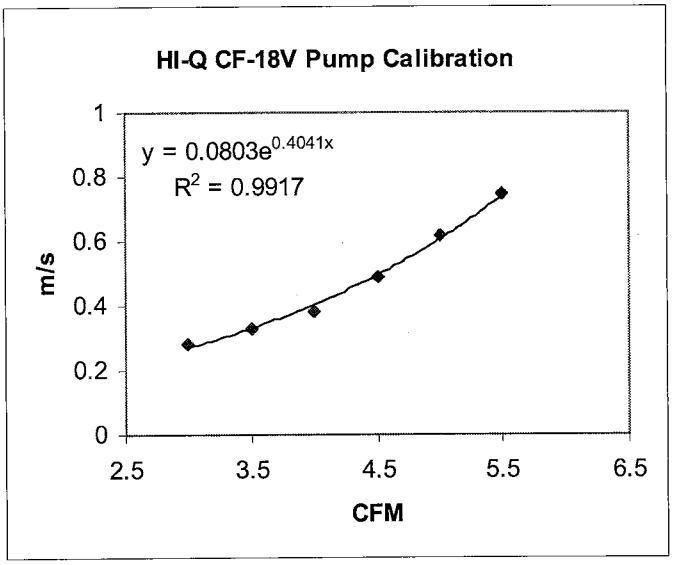

A conversion from CFM to m/s for the intermediate values uses the equation:

$$m/s = 0.0803e^{0.4041 \times CFM}$$

Acid Gas Pump Flow Meter Corrections

The flow meters used with the acid gas pumps are factory calibrated for flow at Standard Temperature and Pressure (STP) of 70 degrees F and 29.92" Hg (at sea level). The correction factors are from HI-Q Environmental Table A-32422 and Table HI-Q Table A-31031.

Pressure Correction Factor (Table A-31031):

$$Pcf = \frac{P_{local}}{P_{base}} = \frac{18.85"\,Hg}{29.92"\,Hg} = 0.63$$

Temperature Correction Factor (Table A-32422):

$$Tcf = \frac{529.67}{459.67 + °F} \times \frac{181.87}{\mu_g}$$, where μ_g is the viscosity of the sampled gas

$$\mu_{air} = \frac{14.58\left(\frac{459.67 - 13°F}{1.8}\right)^{3/2}}{110.4 + \left(\frac{459.67 - 13°F}{1.8}\right)} = 159$$

$$Tcf = \frac{529.67}{459.67 - 13°F} \times \frac{181.87}{159} = 1.36$$

Correction Factor, CF:

$$CF = Tcf \times Pcf = 0.86$$

Gilmont Instruments Flow Meter Calibration (from Scale to L/min)

Scale	Flow air (slpm)
0	0.00
5	2.99
10	6.04
15	8.27
20	11.31
25	14.65
30	18.34
35	21.93
40	26.00
45	29.98

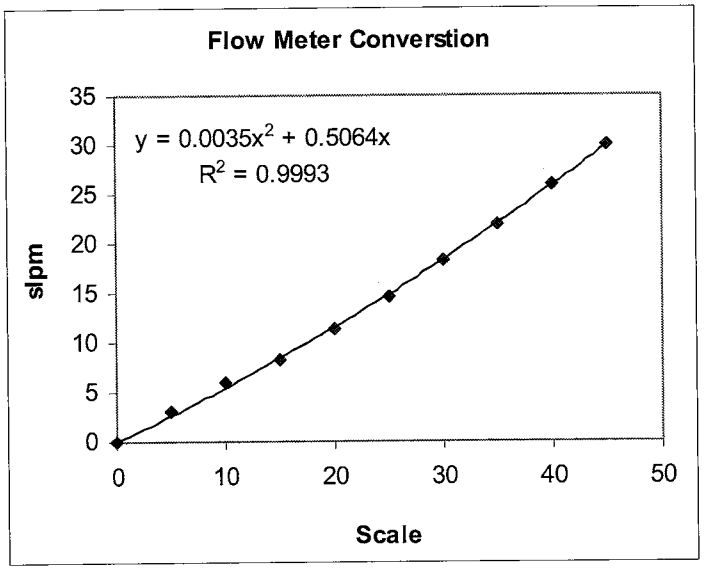

APPENDIX C: Radionuclide Data

TABLE C.1: ^{210}Po Countings and Activities

Sample	Sample Date	Counting Date	Δt (days)	Counts	Counting Time (sec)	Measured Activity (sec)	BG (cps)[1]	Corrected Activity (cps)[2]	Yield[3]	**(^{210}Po) (Bq)**	**(^{210}Po)° (Bq)**
E9915	10-Dec-99	22-Dec-99	12	73527	58740	1.3	3.3E-04	1.3	19.6%	**12769**	**13561**
E9918	11-Dec-99	21-Dec-99	10	33800	21900	1.5	5.0E-04	1.5	19.8%	**15585**	**15600**
E9921	11-Dec-99	29-Dec-99	18	5296	166620	0.0	5.0E-04	0.0	19.8%	**316**	**316**
E9926	12-Dec-99	21-Dec-99	9	112770	21900	5.1	3.3E-04	5.1	18.5%	**55665**	**55716**
E9927	13-Dec-99	28-Dec-99	15	130	253560	0.0	5.8E-04	0.0	20.5%	**0**	**0**
E9930	13-Dec-99	21-Dec-99	8	26785	21960	1.2	3.3E-04	1.2	19.6%	**12443**	**12455**
E9931	13-Dec-99	22-Dec-99	9	97201	58800	1.7	5.0E-04	1.7	19.8%	**16693**	**16709**
E9936	14-Dec-99	28-Dec-99	14	40148	77160	0.5	3.3E-04	0.5	18.5%	**5621**	**5627**
E9939	14-Dec-99	27-Dec-99	13	51413	27240	1.9	1.7E-04	1.9	19.7%	**19160**	**19179**

[1]Background determined by counting for 24 hours with no sample.

[2]Corrected Activity is measured filter activity after background counts and blank values have been removed.

[3]Indicates the percentage of total decays detected by the counter. Yield is determined by counting a known-age alpha source.

TABLE C.2: ^{210}Pb Countings and Activities

Sample	Collection	Counting Date	Δt (days)	Counts	Counting Time (sec)	Measured Activity (cps)	Corrected Activity (cps)[1]	**(^{210}Pb) (mBq)**	**(^{210}Pb)° (mBq)**
E99-15	10-Dec-99	27-Apr-00	138	1186	21600	0.055	4.14E-02	**188**	**190**
E99-18	11-Dec-99	27-Apr-00	138	1478	21600	0.068	5.49E-02	**250**	**253**
E99-21	11-Dec-99	1-May-00	142	1177	86400	0.014	1.04E-04	**0**	**0**
E99-26	12-Dec-99	28-Apr-00	138	4883	21600	0.226	2.13E-01	**966**	**978**
E99-27	13-Dec-99	3-May-00	142	1168	86400	0.014	0.00E+00	**0**	**0**
E99-30	13-Dec-99	27-Apr-00	136	1834	43200	0.042	2.89E-02	**132**	**133**
E99-31	13-Dec-99	2-May-00	141	3811	43200	0.088	7.47E-02	**340**	**344**
E99-36	14-Dec-99	28-Apr-00	136	1605	64800	0.025	1.13E-02	**51**	**52**
E99-39	14-Dec-99	2-May-00	140	1600	21600	0.074	6.06E-02	**275**	**279**

The beta counter detects a background activity of 0.013 counts/second; background determined by counting for 24 hours with no sample.

The beta counter detects 22% of total beta emissions from a filter, as determined by measuring counts on a known-age beta source.

[1]Corrected Activity is measured filter activity after background counts and blank values have been removed.

TABLE C.3: ^{210}Bi Countings and Activities

Sample	Collection	Counting Date	Δt (days)	Counts	Counting Time (sec)	Measured Activity (cps)	Corrected Activity (cps)[1]	β **Activity (mBq)**	(^{210}Bi)° **(mBq)**
E99-15	10-Dec-99	22-Dec-99	12	3972	21600	0.184	0.17	**777**	**3364**
E99-18	11-Dec-99	23-Dec-99	12	21723	86400	0.251	0.24	**1086**	**4853**
E99-21	11-Dec-99	28-Dec-99	17	1430	86400	0.017	0.00	**18**	**185**
E99-26	12-Dec-99	23-Dec-99	11	47002	43200	1.088	1.08	**4888**	**18232**
E99-27	13-Dec-99	3-Jan-00	21	1216	108000	0.011	0.00	**0**	**0**
E99-30	13-Dec-99	25-Dec-99	12	3745	21600	0.173	0.16	731	3268
E99-30	13-Dec-99	29-Dec-99	16	2563	21600	0.119	0.11	482	3101
E99-30							**average:**	**607**	**3185**
E99-31	13-Dec-99	29-Dec-99	16	5547	21600	0.257	0.24	**1110**	**7192**
E99-36	14-Dec-99	30-Dec-99	16	2512	64800	0.039	0.03	**119**	**641**
E99-39	14-Dec-99	29-Dec-99	15	6031	43200	0.140	0.13	**577**	**2750**

The beta counter detects a background activity of 0.013 counts/second; background determined by counting for 24 hours with no sample.

The beta counter detects 22% of total beta emissions from a filter; yield determined by measuring counts on a known-age beta source.

[1]Corrected Activity is measured filter activity after background counts and blank values have been removed.

APPENDIX D
Table D.1: Sulfur Concentrations
4M NaOH impregnated 47 mm Whatman 41 filters

Sample	Sulfate (ppm)	S (ppm)	µg S/filter	µg S/m^3 air	µg S/m^3 air
E99-1A	0.3873	0.1291	15.49	13.33	
E99-1B	0.9678	0.3226	38.71	33.32	
E99-1C	0.316	0.1053	12.64	10.88	57.5
E99-3A	0.2958	0.0986	11.83	28.16	
E99-3B	1.4734	0.4912	58.94	140.27	
E99-3C	1.1632	0.3878	46.53	110.74	279.2
E99-5A	0.2092	0.0697	8.37	10.08	
E99-5B	18.1123	6.0383	724.49	872.58	
E99-5C	1.2875	0.4292	51.50	62.03	944.7
E99-7A	0.3539	0.1180	14.16	22.23	
E99-7B	4.1792	1.3933	167.17	262.47	
E99-7C	2.2892	0.7632	91.57	143.77	428.5
E99-9A	0.3864	0.1288	15.46	BLANK	
E99-9B	2.2952	0.7652	91.81	BLANK	
E99-9C	1.6223	0.5408	64.89	BLANK	
E99-40A	0.2833	0.0944	11.33	BLANK	
E99-40B	1.8177	0.6060	72.71	BLANK	
E99-40C	3.7883	1.2630	151.53	BLANK	

Table D.2: Sulfur Concentrations
3M LiOH impregnated 47mm Whatman 41 filters

Sample	Sulfate (ppm)	S (ppm)	µg S/filter	µg S/m^3 air	µg S/m^3 air
E99-02A	0.0544	0.0181	2.18	2.33	
E99-02B	-0.0976	-0.0325	-3.90	-4.17	
E99-02C	0.7739	0.2580	30.96	33.10	31.25
E99-04A	0.0846	0.0282	3.38	3.62	
E99-04B	1.4547	0.4850	58.19	62.22	
E99-04C	0.5474	0.1825	21.90	23.41	89.25
E99-06A	0.0617	0.0206	2.47	2.54	
E99-06B	2.1283	0.7095	85.13	87.54	
E99-06C	0.8375	0.2792	33.50	34.45	124.52
E99-10A	0.0142	0.0047	0.57	BLANK	
E99-10B	-0.1299	-0.0433	-5.20	BLANK	
E99-10C	0.1344	0.0448	5.38	BLANK	
E99-20A	0.392	0.1307	15.68	4.56	
E99-20B	28.1169	9.3737	1124.68	326.96	
E99-20C	17.1988	5.7338	687.95	200.00	531.5
E99-23A	0.1111	0.0370	4.44	2.41	
E99-23B	14.7625	4.9216	590.50	320.20	
E99-23C	2.2483	0.7495	89.93	48.77	371.4
E99-25A	0.0783	0.0261	3.13	3.62	
E99-25B	5.7828	1.9279	231.31	267.36	
E99-25C	14.1828	4.7283	567.31	655.73	926.7
E99-32A	-0.0121	-0.0040	-0.48	0.00	
E99-32B	2.1942	0.7315	87.77	103.49	
E99-32C	0.4936	0.1646	19.74	23.28	126.8
E99-34A	-0.0068	-0.0023	-0.27	0.00	
E99-34B	1.2604	0.4202	50.42	59.45	
E99-34C	0.3553	0.1185	14.21	16.76	76.2

Table D.3: Sulfur Concentrations
1M Zn Acetate impregnated 47mm Whatman 41 filters

Sample	Sulfate (ppm)	S (ppm)	µg S/filter	µg S/m^3 air	µg S/m^3 air
E99-08A	0.0394	0.0131	1.58	1.62	
E99-08B	3.0444	1.0150	121.78	125.22	
E99-08C	0.9171	0.3057	36.68	37.72	164.56
E99-11A	-0.0078	-0.0026	-0.31	BLANK	
E99-11B	-0.0088	-0.0029	-0.35	BLANK	
E99-11C	0.0034	0.0011	0.14	BLANK	
E99-12A	0.0638	0.0213	2.55	2.95	
E99-12B	3.2492	1.0832	129.97	150.28	
E99-12C	1.7129	0.5711	68.52	79.22	232.5
E99-17A	0.1333	0.0444	5.33	6.17	
E99-17B	8.1947	2.7320	327.79	379.01	
E99-17C	0.7613	0.2538	30.45	35.21	420.4
E99-29A	0.0321	0.0107	1.28	1.58	
E99-29B	0.6226	0.2076	24.90	30.74	
E99-29C	0.796	0.2654	31.84	39.30	71.6
E99-37A	0.1105	0.0368	4.42	4.82	
E99-37B	7.7513	2.5842	310.05	338.03	
E99-37C	0.7307	0.2436	29.23	31.87	374.7

Table D.4: Sulfur Concentrations
1M Zn Acetate impregnated 37mm Millipore cellulose pads

Sample	Sulfate (ppm)	S (ppm)	µg S/filter	µg S/m^3 air	µg S/m^3 air
E99-13B	0.7026	0.2342	14.05	15.93	
E99-13C	0.5254	0.1752	10.51	11.91	27.8
E99-14B	0.0163	0.0054	0.33	BLANK	
E99-14C	-0.0132	-0.0044	-0.26	BLANK	
E99-16B	21.674	7.2258	433.48	463.67	
E99-16C	17.5147	5.8391	350.29	374.69	838.4
E99-19B	32.8094	10.9381	656.19	181.88	
E99-19C	14.7564	4.9195	295.13	81.80	263.7
E99-22B	5.168	1.7229	103.36	51.59	
E99-22C	3.2952	1.0986	65.90	32.89	84.5
E99-24B	9.7136	3.2384	194.27	207.80	
E99-24C	22.3827	7.4620	447.65	478.83	686.6
E99-28B	3.2212	1.0739	64.42	82.62	
E99-28C	0.0536	0.0179	1.07	1.37	84.0
E99-33B	2.1861	0.7288	43.72	47.67	
E99-33C	0.0587	0.0196	1.17	1.28	48.9
E99-35B	1.2836	0.4279	25.67	27.99	
E99-35C	0.1686	0.0562	3.37	3.68	31.7
E99-38B	15.4518	5.1514	309.04	336.92	
E99-38C	1.6087	0.5363	32.44	36.77	96.2

Appendix E.1a: Erebus Sulfur Dioxide filters, December 2000

Sample	Date	A filt	B & C filters	Size (mm)	Start Time[1]	Stop Time[1]	Total Time (min)	Pump Start (scale)[2]	Pump Stop (scale)[2]	Flow Start (lpm)[3]	Flow Stop (lpm)[3]	Volume (liters)	Volume (m^3)	Wind (knots)	Wind Dir	Plume Strength[4]	Sample
E00-02	10-Dec-00	Z2.0	1Zn	47	1439	1501	22	20	20	12	12	259	0.26	3	S	7/10	E00-02
E00-03	10-Dec-00		1Zn	37	1440	1501	21	17	17	10	10	202	0.20	3	S	7/10	E00-03
E00-05	10-Dec-00	Z2.0	1Zn	47	1504	1535	21	20	22	12	13	259	0.26	3	S	7/10	E00-05
E00-06	10-Dec-00		1Zn	37	1505	1535	20	17	17	10	10	192	0.19	3	S	7/10	E00-06
E00-08	11-Dec-00	Z2.0	1Zn	47	1047	1107	20	20	20	12	12	236	0.24	6	E,S	8/10	E00-08
E00-09	11-Dec-00		1Zn	37	1047	1107	20	17	17	10	10	192	0.19	6	E,S	8/10	E00-09
E00-11	11-Dec-00	Z2.0	1Zn	47	1114	1134	20	20	20	12	12	236	0.24	6	E,S	8/10	E00-11
E00-12	11-Dec-00		1Zn	37	1112	1132	20	17	17	10	10	192	0.19	6	E,S	8/10	E00-12
E00-14	12-Dec-00	Z2.0	3Li	47	1240	1301	21	21	21	12	12	259	0.26	1	S	8/10	E00-14
E00-15	12-Dec-00		1Zn	37	1240	1301	21	19	18	11	10	219	0.22	1	S	8/10	E00-15
E00-17	12-Dec-00	Z2.0	3Li	47	1634	1656	22	21	20	12	12	265	0.27	1	S	8/10	E00-17
E00-18	12-Dec-00		1Zn	37	1634	1656	22	18	18	10	10	223	0.22	1	S	8/10	E00-18
E00-20	13-Dec-00	Z2.0	3Li	47	1531	1552	21	20	20	12	12	248	0.25	1	S,E	5/10	E00-20
E00-21	13-Dec-00		1Zn	37	1531	1552	21	20	18	11	10	225	0.22	1	S,E	5/10	E00-21
E00-23	13-Dec-00	Z2.0	3Li	47	1559	1619	20	20	20	11	11	225	0.22	1	S,E	5/10	E00-23
E00-24	13-Dec-00		1Zn	37	1559	1619	20	18	18	10	10	203	0.20	1	S,E	5/10	E00-24
E00-26	14-Dec-00	Z2.0	3Li	47	1322	1343	21	20	20	11	11	236	0.24	3	S	5/10	E00-26
E00-27	14-Dec-00		1Zn	37	1322	1343	21	19	18	11	10	219	0.22	3	S	5/10	E00-27
E00-29	14-Dec-00	Z2.0	1Zn	47	1348	1408	20	20	20	11	11	225	0.22	3	S	5/10	E00-29
E00-30	14-Dec-00		1Zn	37	1348	1408	20	18	18	10	10	203	0.20	3	S	5/10	E00-30
E00-32	15-Dec-00	Z2.0	1Zn	47	1244	1306	22	19	20	11	11	241	0.24	8	S	5/10	E00-32
E00-33	15-Dec-00		1Zn	37	1244	1306	22	18	18	10	10	223	0.22	8	S	5/10	E00-33
E00-35	15-Dec-00	Z2.0	1Zn	47	1312	1334	22	20	20	11	11	247	0.25	8	S	5/10	E00-35
E00-36	15-Dec-00		1Zn	37	1312	1334	22	18	18	10	10	223	0.22	8	S	5/10	E00-36
E00-38	16-Dec-00	Z2.0	1Zn	47	1351	1417	26	20	20	12	12	306	0.31	8	S	3/10	E00-38
E00-39	16-Dec-00		1Zn	37	1351	1417	26	18	18	10	10	264	0.26	8	S	3/10	E00-39
E00-41	16-Dec-00		1Zn	47	1421	1446	25	20	20	12	12	295	0.29	8	S	3/10	E00-41
E00-42	16-Dec-00		1Zn	37	1421	1446	25	18	17	10	10	247	0.25	8	S	3/10	E00-42
E00-44	17-Dec-00	Z2.0	3Li	105	1552	1629	37	32	30	20	18	706	0.71	1	S	0/10	E00-44
E00-45	17-Dec-00	Z2.0	3Li	105	BLANK												E00-45
E00-46	17-Dec-00		1Zn	37	1552	1629	37	17	17	10	10	356	0.36	1	S	0/10	E00-46
E00-47	17-Dec-00		1Zn	37	BLANK												E00-47

Appendix E.1b: Erebus Sulfur Dioxide filters, December 2000

Sample	Date	A filt	B & C filters	Size (mm)	Start Time[1]	Stop Time[1]	Total Time (min)	Pump Start (scale)[2]	Pump Stop (scale)[2]	Flow Start (lpm)[3]	Flow Stop (lpm)[3]	Volume (liters)	Volume (m^3)	Wind (knots)	Wind Dir	Plume Strength[4]	Sample
E00-49	19-Dec-00		1Zn	37	1226	1247	21	19	18	11	10	219	0.22	10	S	10/10	E00-49
E00-51	19-Dec-00		1Zn	37	1249	1310	21	18	18	10	10	213	0.21	10	S	10/10	E00-51
E00-52	19-Dec-00	Z2.0	3Li	105	1229	1313	44	30	30	18	18	799	0.80	10	S	10/10	E00-52
E00-54	21-Dec-00		1Zn	37	1725	1753	28	19	18	11	10	292	0.29	nd	nd	nd	E00-54
E00-56	21-Dec-00		1Zn	37	1755	1818	23	17	18	10	10	227	0.23	nd	nd	nd	E00-56
E00-57	21-Dec-00	Z2.0	3Li	105	1723	1818	55	32	30	20	18	1050	1.05	nd	nd	nd	E00-57
E00-59	22-Dec-00		1Zn	37	1714	1737	23	18	18	10	10	234	0.23	nd	nd	nd	E00-59
E00-60	22-Dec-00	Z2.0	3Li	105	1713	1739	26	29	29	18	18	457	0.46	nd	nd	nd	E00-60
E00-61	22-Dec-00	Z2.0	1Zn	47	BLANK									n/a	n/a	n/a	E00-61
E00-62	22-Dec-00	Z2.0	3Li	47	BLANK									n/a	n/a	n/a	E00-62
E00-63	04-Jan-01	Z2.0	1Zn	47	BLANK									n/a	n/a	n/a	E00-63
E00-64	04-Jan-01	Z2.0	3Li	47	BLANK									n/a	n/a	n/a	E00-64
E00-65	04-Jan-01		1Zn	37	BLANK									n/a	n/a	n/a	E00-65
E00-66	04-Jan-01	Z2.0	3Li	105	BLANK									n/a	n/a	n/a	E00-66
E00-68	04-Jan-01		1Zn	37	1327	1347	20	18	19	10	11	208	0.21	n/a	n/a	n/a	E00-68
E00-70	04-Jan-01		1Zn	37	1513	1612	61	18	18	10	10	619	0.62	n/a	n/a	n/a	E00-70

Z2.0: Zefluor Teflon filter, 2 micron pore size ; 3Li: 3M LiOH prepared 18 Oct 2000; 1Zn: 1M Zn acetate prepared 18 Oct 2000

[1]All times McMurdo local summer time

[2]Scaled flow corrected for Erebus barometric pressure and temperature using HI-Q Environmental Tables A-31031 and A-32422 (Appendix B).

[3]Liters/minute calculated from flowmeter scale using Gilmont Instruments flowmeter calibration data (Appendix B).

[4]Plume strength indicates concentration of the plume on a 1-10 scale with 10 being the most concentrated.

n/a: no data due to BLANK filter

nd: no data recorded for these samples

Appendix E.2: Erebus Suflur Dioxide filters, December 2001

Sample	Date	A filt	B & C filters	Size (mm)	Start Time[1]	Stop Time[1]	Total Time (min)	Pump Start (scale)[2]	Pump Stop (scale)[2]	Flow Start (lpm)[3]	Flow Stop (lpm)[3]	Volume (liters)	Volume (m^3)	Wind (knots)	Wind Dir	Plume Strength[4]	Sample
E01-02	08-Dec-01	Z2.0	1Zn	101	1224	1254	30	20	21	11	12	354	0.35	15	S	7/10	E01-02
E01-03	08-Dec-01		1Zn	37	1237	1248	11	12	12	7	7	72	0.07	15	S	7/10	E01-03
E01-05	11-Dec-01		1Zn	37	1351	1413	18	14	18	8	10	159	0.16	0	nil	3/10	E01-05
E01-07	11-Dec-01		1Zn	36	1416	1437	21	18	18	10	10	213	0.21	0	nil	3/10	E01-07
E01-08	11-Dec-01	Z2.0	1Zn	101	1354	1437	43	21	21	12	12	531	0.53	0	nil	3/10	E01-08
E01-10	13-Dec-01		1Zn	37	1317	1332	15	18	18	10	10	152	0.15	25	S	10/10	E01-10
E01-11	13-Dec-01	Z2.0	1Zn	47	1310	1330	20	18	18	10	10	203	0.20	25	S	10/10	E01-11
E01-12	18-Dec-01		1Zn	37	BLANK									n/a	n/a	n/a	E01-12
E01-13	18-Dec-01	Z2.0	1Zn	47	BLANK									n/a	n/a	n/a	E01-13

Z2.0: Zefluor Teflon filter, 2 micron pore size ; 1Zn: 1M Zn acetate prepared 18 Oct 2001
[1]All times McMurdo local summer time
[2]Scaled flow corrected for Erebus barometric pressure and temperature using HI-Q Environmental Tables A-31031 and A-32422 (Appendix B).
[3]Liters/minute calculated from flowmeter scale using Gilmont Instruments flowmeter calibration data (Appendix B).
[4]Plume strength indicates concentration of the plume on a 1-10 scale with 10 being the most concentrated.
n/a: no data due to BLANK filter